ANALYSIS OF DROPLET IMPACT ON A LIQUID POOL

by

Radhika Arvind Bhopatkar

A Thesis

Submitted to the Faculty of Purdue University

In Partial Fulfillment of the Requirements for the degree of

Master of Science in Mechanical Engineering

School of Mechanical Engineering

West Lafayette, Indiana

August 2020

THE PURDUE UNIVERSITY GRADUATE SCHOOL
STATEMENT OF COMMITTEE APPROVAL

Dr. Paul E. Sojka, Chair
School of Mechanical Engineering

Dr. Jun Chen
School of Mechanical Engineering

Dr. Terrence Meyer
School of Mechanical Engineering

Approved by:
Dr. Nicole Key

Dedicated to my God, family, friends and advisor

ACKNOWLEDGMENTS

I would like to take this opportunity to thank everyone who have helped and supported me in different ways during my master's curriculum. Without them I wouldn't have been able to grow academically, professionally and personally.

Firstly, I would like to express my deep gratitude towards my advisor Prof. Paul E. Sojka who has always supported me and inspired me to gain a deeper understanding in whatever I pursue. He has been always a great mentor and a friend who has guided me throughout my master's program. Over the course of my research work he has always helped me to understand various experimental and theoretical concepts which have immensely helped me progress towards my thesis work. I sincerely thank him for always being there for me and being a pillar of support for me throughout since August 2018.

I would also like to thank my Committee members Prof. Terrence Meyer and Prof. Jun Chen for their time and support. I would also take this opportunity to thank Prof. Jun Chen and his group for supporting me in the lab.

I would especially like to thank Dayna Obenauf, Dongyun Shin, LongChao Yao, Vishnu Radhakrishna, Weixiao Shang, and Yijie Wang, for their active support and help in my research proceedings.

Last but not the least I wish to thank my parents, grandparents and my friends Akshay, Aditya, Darshit, Deepti, Himal, Rashmi and Siddhant who have stood by me in every situation and made my journey at Purdue University a memorable one!

TABLE OF CONTENTS

LIST OF TABLES

LIST OF FIGURES

NOMENCLATURE

d	INITIAL DROPLET DIAMETER
DIH	DIGITAL INLINE HOLOGRAPHY
h	THICKNESS OF POOL
Oh	OHNESORGE NUMBER
pdfs	PROBABILITY DENSITY FUNCTION
V	DROPLET VELOCITY
We	WEBER NUMBER
δ	NON-DIMENSIONAL FILM/POOL THICKNESS
μ	DYNAMIC VISCOSITY
ρ	DENSITY
σ	SURFACE TENSION

ABSTRACT

Secondary atomization is very important in applications like IC engine and aircraft engine performance, agricultural sprays, and inkjet printing to name a few. In case of IC engines and aircraft engines, a good understanding of the modes of secondary atomization and the resultant drop size can contribute to improving the fuel injection and hence the efficiency of the engine. Similarly, with the help of appropriate secondary atomization desired agro-spray quality, ink usage and print quality can be achieved which would optimize the usage of chemicals and ink respectively and avoid any harmful effects on the environment.

One of the reasons for secondary atomization that occurs very often in most of the spray applications is the drop impact on a solid or liquid surface. Especially it is cardinal to understand the impact of a drop on a liquid film since even in case of impact of liquid drops on a solid surface ultimately the drops that are injected at a later time are going have a target surface as a thin liquid film on the solid base due to the accumulation of the previously injected drops. Analysis of drop impact on a liquid film with non-dimensional thickness ranging from 0.1 to 1 has been done thoroughly before (Cossali *et al.,* 2004, Vander Waal *et al.,* 2006, Moreira *et al.,* 2010), however, analysis of drop impact on a liquid film with non-dimensional thickness greater than 1 is still in a rudimentary stage. This work focuses on determining the probability density functions for the secondary drop sizes for drops produced in case of drop impact on a liquid film while varying the h/d ratio beyond 1. The experimental set-up used to study drop impact includes a droplet generator and DIH system as mentioned in, Yao *et al.* (2017). The DIH set-up includes a CW laser, spatial filter, beam expander and a collimator as adapted from Guildenbecher *et al.* (2016). The height of drop impact is varied to vary the impact *We*, by adjusting the syringe height. Three fluids- DI-Water, ethanol and glycerol are tested for examining the effect of viscosity on the resultant drop sizes. Results are plotted with respect to viscosity, impact *We* and the non-dimensional film thickness, as the fragmentation of drops is directly associated to these parameters. Results indicate that majority of the secondary droplets lie in the size range of 25 µm to 50 µm. It is also observed that the tendency of secondary atomization from crown splashing increases with the increase in *We* and decreases with increase in *Oh.*

1. INTRODUCTION

Raindrops falling on earth's surface, a jet from a faucet, coating on a surface using a spray, fire extinction using water sprays, fuel injection in gas turbine and IC engines, along with sprays of water in farms for proper irrigation are things that we see in our daily life. We can see the phenomenon that occurs when a drop impact takes place on a solid or a liquid surface, however, only at a very macroscopic level. It is indeed important to examine and understand the dynamics behind the drop impact phenomenon on a microscopic scale in many applications so as to optimize the spray and get the desired final result from the impinging spray.

Over the last fifty years there has been considerable research into drop impact on solid and liquid surfaces and it is still ongoing. Especially it is cardinal to understand the impact of a drop on a liquid film since even in case of impact of liquid drops on a solid surface ultimately the drops that are injected at a later time are going to have a target surface as a thin liquid film on the solid base due to the accumulation of the previously injected drops.

1.1 Thesis Focus / Motivation

With the increasing number of applications involving liquid impact on a liquid film it has become important to understand the phenomenon both in more detail and in a broader sense, incorporating a variety of operating/ fluid conditions. Previous studies involve examination of the impact phenomenon from the dynamics point of view only. However, there has been very less research in determining the probability density functions for the drop sizes for drops produced in every regime of drop impact on a liquid film. Also, analysis of droplet impact on a liquid film with non-dimensional thickness ranging from 0.1 to 1 has been covered (Cossali *et al.*, 2004, Vander Wal *et al.*, 2006, Moreira *et al.*, 2010). However, analysis of drop impact on a liquid film with non-dimensional thickness greater than 1 is still in a rudimentary stage. Empirical relations for finding the threshold K (Sommerfeld parameter) have also been established for non-dimensional film thicknesses 0.1 to 1. Thus, this work will primarily focus on varying the δ = h/d ratio beyond 1 (δ = 5.67). The impact velocity and fluid viscosity are varied to study the corresponding effect of

changing *We* and *Oh* on the droplet impact phenomenon. The obtained results are used to develop *pdfs* for the diameter, volume, and velocity of the secondary drops.

1.2 Non-dimensional quantities

Droplet impact on a liquid film/pool is governed by a number of parameters, including initial droplet size, liquid physical properties, impact velocity, impact angle (Lee *et al*., 2011). The influence of these parameters can be understood by combining them to give non-dimensional terms *We* and *Oh* and δ. *We* gives the relation between inertial and surface tension forces whereas *Oh* gives the relation between viscous forces and inertial plus surface tension forces. δ is the non-dimensional thickness of the film or the pool.

$$We = \frac{\rho V^2 d}{\sigma} \qquad Oh = \frac{\mu}{\sqrt{\rho \sigma d}} \qquad \delta = h / d$$

In the following sections different regimes occurring during the drop impact and the influence of non-dimensional quantities on the impact will be explained and compared to the work presented by other researchers previously. Conclusions will be drawn from the data and a summary of findings presented.

2. LITERATURE REVIEW

2.1 Overview

During the course of studying the dynamics of drop impact on liquid film researchers have used fluids like water, hexadecane, heptane, propanol, methanol, glycerol, FC-2 (Vander Wal *et al.*, 2006), to name a few. These fluids were chosen because they cover a wide range of viscosity which helps to determine its effect. Weber number was varied by adjusting the impact velocity with values as high as 5100 (Pan and Hung, 2010). The range of Re considered with within this literature review is $200<Re<16000$ (Josserand *et al.,* 2016). Viscosities up to 10000 mm^2/s have been considered previously for in depth analysis (Kittel *et al.,* 2007).

2.2 Regimes occurring during drop impact on a liquid film

Drop impact on a liquid film is a complex phenomenon and consists of many different regimes depending on the range of *We* and non-dimensional film thickness used. A drop can coalesce, bounce, rebound or splash with the liquid film (Rein *et al.*, 1996, Cossali *et al.*, 1999). The following subsections will give a detailed explanation of the same.

2.2.1 Coalescence/Deposition

This phenomenon occurs at low impact velocity which leads to just the spreading of the droplet after its impact on the liquid surface without any jetting. The correlation which represents the threshold between deposition and splashing is given by $K = (We \cdot Oh^{-0.4}) = (Re \cdot We^2)^{0.4}$ (Yang *et al.,* 2017). Cossali *et al.* (1997), studied the deposition regime with glycerol water mixtures to further develop the splash-deposition boundary. It was identified by Yarin and Weiss (1995) that splash was a function of viscosity, surface tension, density and drop frequency and hence these properties were essential to be considered while determining the deposition-splash boundary. The effect of Froude number on the splash-deposition boundary determination has been considered in the previous studies by Rodriguez and Messler (1985). Josserand and Zaleski (2016) have also done a numerical study to facilitate the prediction of transition between deposition and splashing phenomenon. In simple terms the spreading of a droplet on the surface is determined by the lamella flow and propagation of the film (Kittel *et al.,* 2017).

2.2.2 Bouncing and Merging

Bouncing of the droplet as it impacts the impact liquid surface is desired in case of internal combustion engines so as to avoid any kind of fuel accumulation which will lead to higher emission of exhaust gases (Tang *et al.*, 2018). Hence, examination of this regime is vital.

Tang *et al.* (2018) have done substantial work in analyzing the bouncing regime by considering a wide range of viscosity- 0.7 to 100 cSt – along with the effect of impact *We*. Tang *et al.* (2018) took the analysis of bouncing and merging regimes to the next level by considering the case of drop impact on a liquid film of comparable thickness and devised the inertial limit which serves as a boundary between bouncing and impact merging. According Tang *et al.* (2018), the inertial limit is the boundary when bouncing phenomenon no longer occurs and what arises is impact merging after *We* exceeds a minimum value. When the kinetic energy is high enough to break the gas layer between the drop and the film then merging of the drop in the film takes place (Tang *et al.*, 2018). Tang *et al.* (2018) also gave a relation for critical velocity at the transition between the bouncing and impact merging of the drops as $U_{p,cr} = \mu R^{1/2} d_{cr}^{-3/2} / \rho$. In general, they observed increasing viscosity leading to the merging phenomenon occurs at a higher *We.* In short, the merging regime is delayed as viscosity is increased.

2.2.3 Prompt Splash

According to Vander Wal *et al.* (2006), prompt splashing means ejection of drops from the rim of the ejecta sheet in the initial stages of crown formation. Vander Wal *et al.* (2006) also had found that as the viscosity increases the tendency of prompt splashing decreases. They drew some important conclusions with regard to the effect of viscosity and surface tension on prompt splashing occurrence by testing with heptane, hexadecane, propanol, methanol etc.

Cossali *et al.* (2005) also identified that formation of crown has three phases viz prompt, crown and splashing and that the splashing is a regime that occurs during the advancement of the crown. It was observed by Cossali *et al.* (2005) that prompt splashing occurs at low *Oh* and low surface tension.

As reported by Josserand and Zaleski *et al.* (2016), prompt splash is defined as the regime that is associated with the ejecta sheet that forms at time t << Uo/d, where Uo is the velocity and d is the diameter of the droplet. Occurrence of prompt splash can contribute to kick start instability by giving additional disturbance (Deegan *et al.*, 2007).

In the initial stage of research, Worthington (1887) considered prompt splashing to be a result of the formation of a compression wave in the drop after its impact on the liquid film. However, in response to the above-mentioned result Yarin and Weiss (1999) had reported that the prompt splash is due to the torus like deformation of the drop due to the inertia effects.

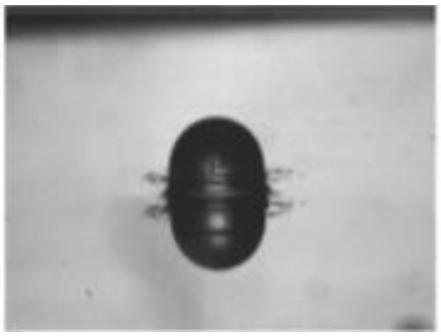

Figure 1: Prompt splash (Banks et al., 2013)

2.2.4 Crown formation

Banks *et al.* (2013), characterized crown formation as the occurrence of capillary wave above the original surface level of the film. Yarin and Weiss (1999) considered crown spreading as a kinematic discontinuity in their shallow water approach. Liang *et al.* (2014) reported that as time increases the crown propagates radially along with the increase in crown height. This outcome was observed for conditions of *We* = 2010, Re = 1168, and non-dimensional film thickness of 0.5. The crown was observed not to be usually cylindrical and the diameter of the external surface was observed to vary with the distance from the upper surface of the film (Coghe *et al.*, 1999). Yarin and Weiss (1995), reported that the crown size has following relation

$D_x = C\ (t\text{-}t_0)^n$

Figure 2: Crown formation (Banks et al., 2013)

2.2.5 Crown Splash

Crown splash occurs at very high impact velocity and at very low viscosity. It was reported by Cossali *et al.* (1997) Vander Wal *et al.* (2006), that splashing is related to the formation of satellite drops from the crown rim. It is also known as delayed splashing and is associated with the later stages of crown expansion. (Cossali *et al.*,1997)

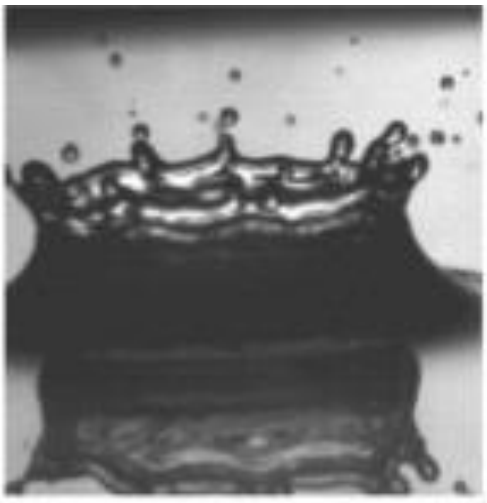

Figure 3: Crown Splashing (Banks et al., 2013)

2.3 Effect of fluid properties on the drop impact on liquid film.

2.3.1 Effect of Ohnesorge number / effect of viscosity

Josserand and Zaleski (2003) had reported that viscosity influences the crown shape by generation of vortices near the neck region and that these vortices determine the inclination of the crown wall. It was observed that the lower viscosity the greater the influence of *We* (Geppert *et al.*, 2017). The film viscosity also affects the maximum crown diameter (Kittel *et al.*, 2016). Geppert *et al.* (2017), also observed through experiments involving two component interactions that a cylindrical crown is formed at the initial time period and a V-shaped crown is formed for a non-dimensional time greater than 2. Low viscosity films were observed to develop a bowl shape first and then a truncated cone shape by Geppert *et al.* (2017). This observation agrees with that of Cossali *et al.* (1997), Vander Wal *et al.* (2006), and Sikalo and Ganic (2006), because all of them considered only low viscosity fluids. Banks *et al.* (2013) had observed that as viscosity increases the crown threshold *We* increases accordingly. Figure 4, shown below illustrates the same. Also, as illustrated by figure 5, there is also a limit imposed up to which the viscosity of the drop can be increased. Up till this limit as viscosity of the drop increases that is the *Oh* of drop increases there is a significant increase in the slope and then beyond this limit it just levels off (Banks *et al.*, 2013). This observation is evident from figure 5 shown below.

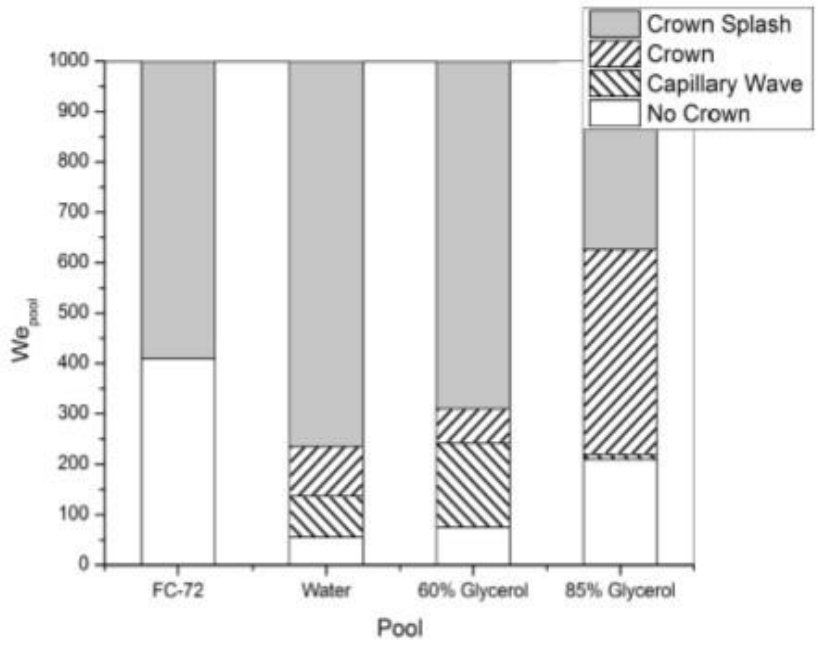

Figure 4: Crown behavior observed when water drops impact varying pools organized by pool viscosity (Banks et al., 2013)

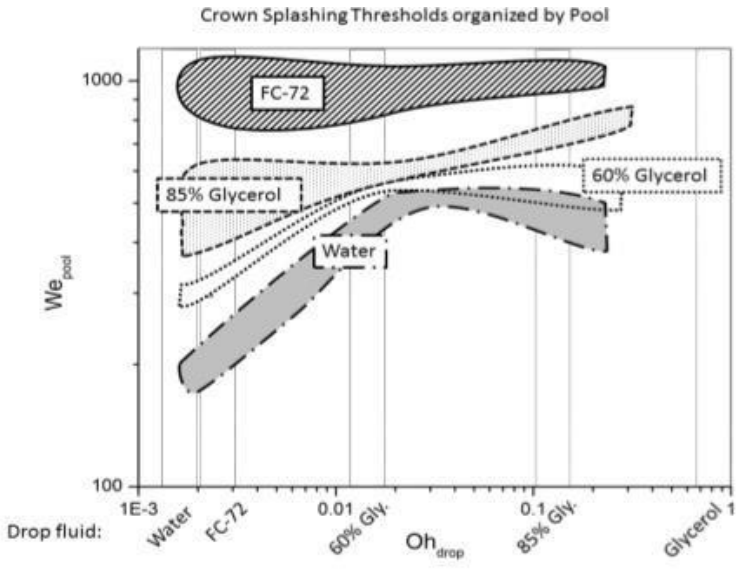

Figure 5: Crown splashing behaviors, organized by film. The regions represent the observed transition from not splashing to consistently splashing. The x-axis includes labels of each drop species with their respective *Oh* range represented by the vertical bars on the graph. (Banks et al., 2013)

The observations of Yang *et al.* (2017), agrees with the observations of Banks *et al.* (2013) that splashing is suppressed with the increase in the fluid viscosity. Further Yang *et al.* (2017) also reported that with increasing viscosity crown wall height reduces, inclination of the crown wall increases, and jetting becomes slower. Figure 6 explains the same.

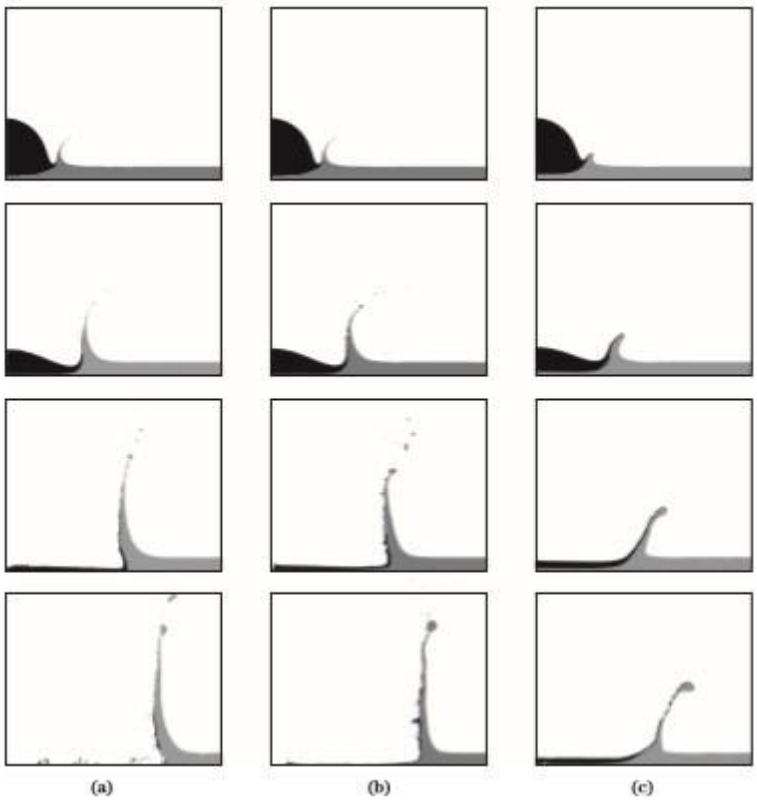

Figure 6: Evolution of crown for various liquid viscosities. T = 0.4,1.0,2.4,4.4 from top row to bottom, respectively. Columns: (a) inviscid; (b) water (Re = 6.96×105); (c) viscosity 100 times larger than that of water (Re = 139) (Yang *et al.*, 2017)

Yang *et al.* (2017) found that the effect of viscosity is negligible on the crown spreading when viscosity is lower, however viscosity significantly influences the crown spreading at times T > 0.4. This is illustrated below.

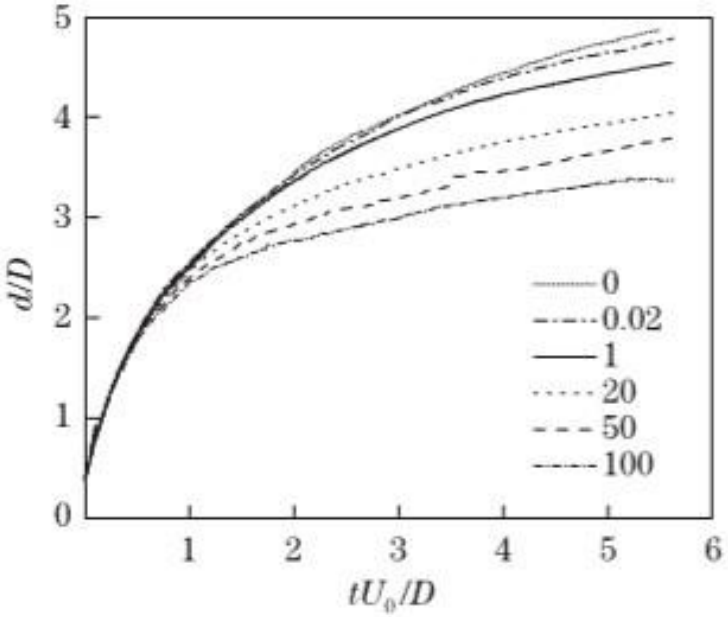

Figure 7: Position of crown as function of time. (Yang *et al.,* 2017)

Vander Wal *et al.* (2006) also reported that viscosity of the fluid affects the mean size and the number of ejected droplets. Increasing viscosity produces a small number of large size droplets. (Vander Wal *et al.,* 2006). Numerical analysis results as obtained by Mukherjee and Abraham (2007) agree with the experimental results of Vander Wal *et al.* (2006) and suggest that when viscosity increases the crown expansion rate and the crown height decreases, accompanied by a delay in the breakup. Findings of Pan and Hung (2010) also agree with the previous studies that increased viscosity impedes the dynamic behavior of the crown.

The viscosity of the film influences the impact outcome only whereas the viscosity of the drop influences the maximum spreading diameter of the crown and maximum spreading time (Kittel *et al.,* 2017). Deegan *et al.* (2008), reported that the ejecta sheet has higher speeds at reduced viscosity. It was also observed that with increasing viscosity the merging phenomenon was delayed because of shifting of the inertial limit to a higher *We* number (Tang *et al.,* 2018).

2.3.2 Effect of *We* number/ effect of impact velocity

Weber number can be altered by changing the height of impact which in turn changes the impact velocity. During the drop penetration phenomenon, the drop penetrates to a higher depth with the increase in the impact inertia (Tang *et al.*, 2018). Cossali *et al.* (2004) studied the various crown parameters like crown diameter, height, and secondary drop diameters with respect to time. Following figures 8 and 9 explicitly mention the crown parameters taken into consideration while analyzing the effect of fluid properties on the drop impact on a liquid film.

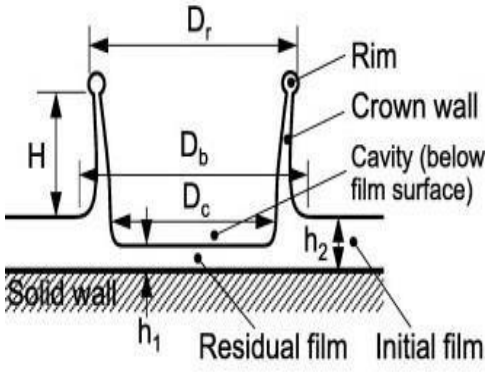

Figure 8: Geometrical parameters of a crown (Kang, 2016)

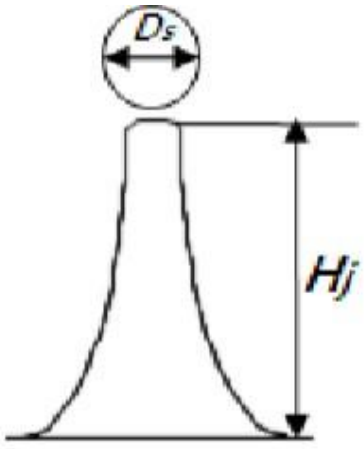

Figure 9: Central jet parameters (Kang, 2016)

Trujillo and Lee (2001) stated that *We* has a negligible influence on the crown radius spreading/evolution and that it is mainly affected by film thickness. Macklin and Metaxas (1976) reported that with higher *We* the crown thickness reduces, and more liquid volume is contained within the crown. However, as against this Cossali *et al.* (2004) showed that crown thickness is independent of the impact velocity and film thickness. Cossali *et al.* (2004) studied the effect of *We* by photographing the drops of millimeter size, considering considered four different *We* Cossali *et al.* (2004) reported that the crown falling velocity during the retraction of the crown also is independent of the *We*. Also, many researchers report that larger difference between the lower and upper diameter of the crown is observed for larger *We*. (Cossali *et al.*, 2004)

Oguz and Prosperetti (1989) first found the occurrence of bubble formation phenomenon which happens due to entrapment of the air in the neck region between the drop and the film. This trapped layer of air forms bubble rings which eventually break up to form bubbles. Thoroddsen *et al.* (2003) also observed this phenomenon with ultra-high-speed video camera. Liang *et al.* (2014) reported with the help of his numerical analysis results that a greater *We* will increase the number of bubble rings. This is because the higher the *We*, the higher the impact velocity which in turn gives less time for contact to be established and hence, air does not get enough time to escape, eventually getting trapped and forming ring like bubbles. (Liang *et al.*, 2014). Figure 10 shows the phenomenon of bubble entrainment.

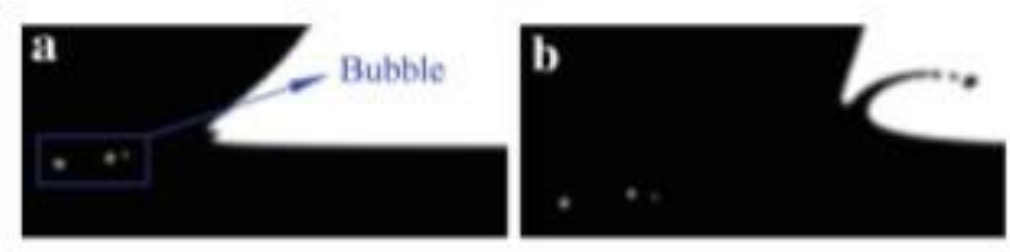

Figure 10: Bubble entrainment of the numerical results. a 0.05ms, b 0.175ms (Liang *et al.*, 2014)

Thus, it can be summarized that there are different regimes that occur at different *We* as shown in figure 11. Thus, to summarize it can be said that the probability of splash occurrence increases with the increasing *We* number. (Banks *et al.*, 2013).

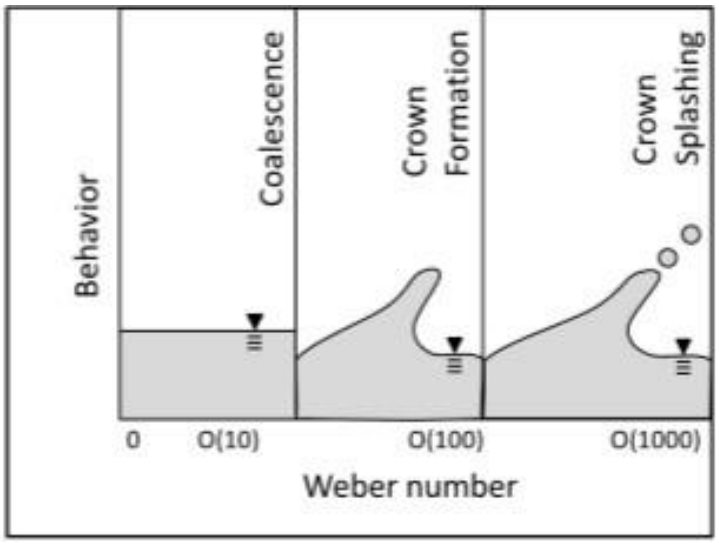

Figure 11: Weber-based regime map for drop impact onto liquid pools, based on past observations (Rein, 1996), fitted to magnitudes found in this study. Diagram depicting the impact outcomes from a horizontal perspective (Banks *et al.*, 2013)

2.3.3 Effect of film thickness

Geometrical parameters of the crown such as diameter and height, as well as the central jet height, are influenced by the impact film thickness (Vander Wal *et al.*, 2006, Liang *et al.*, 2014). Liang *et al*. (2014) reported that crown diameter can be increased by reducing the film thickness. Vander Wal *et al.* (2006) found that for intermediate film thickness prompt splash occurrence decreases for heptane, decane, hexadecane, DI-Water, 30% glycerol, methanol, n-propanol, butanol.

Cossali *et al.* (1999) concluded that non-dimensional crown thickness is independent of film thickness. The maximum crown height and the time at which it is attained depend on the drop impact velocity and the influence of the film thickness appears to be very weak (Cossali *et al.*, 1999). In contrast, Kang (2016) observed that increasing the film thickness while keeping the impact velocity same increases the height of the central jet and decreases the height of the crown. Secondary atomization is seen to occur in the case of decreased film thickness and/or increased impact velocity. Following figure 12 and 13 illustrate the same.

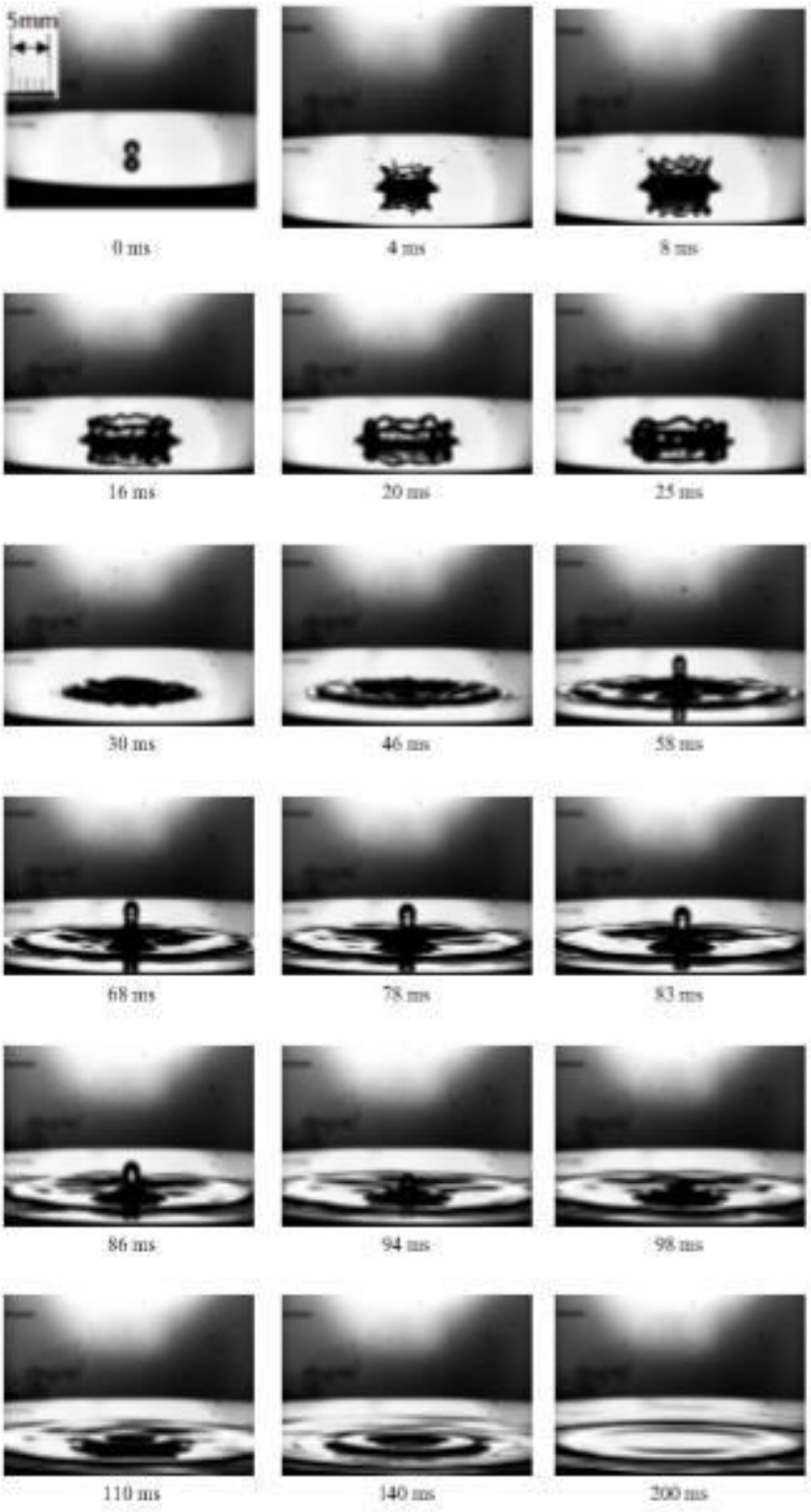

Figure 12: Behavior of an impacting droplet onto a liquid film, for the case of h = 2 mm, V=2.75 m/s. (Kang, 2016)

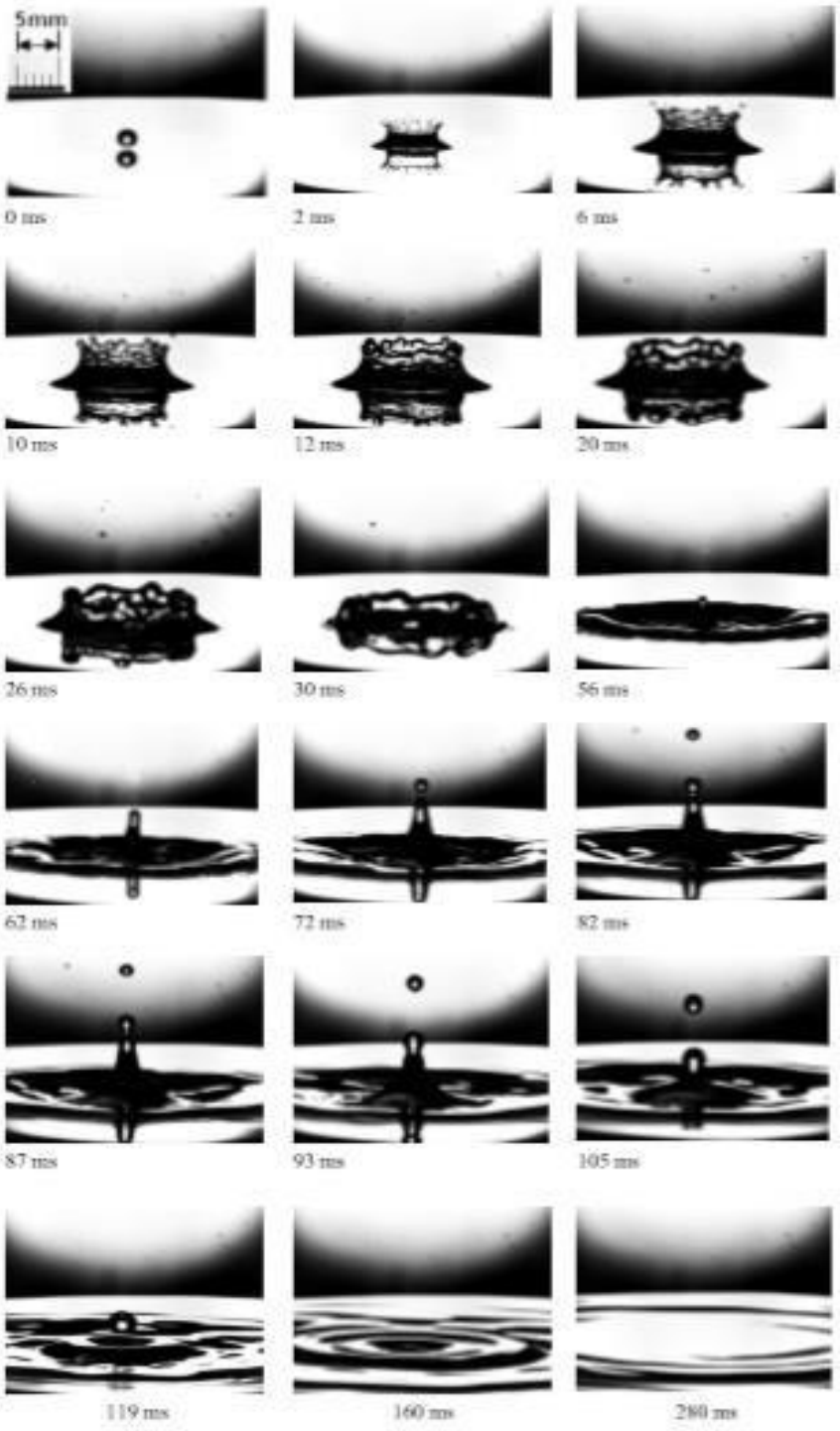

Figure 13: Behavior of an impacting droplet onto a liquid film, for the case of h = 2 mm, V=4.1 m/s. (Kang, 2016)

The following figure 14 illustrates the various regimes as a function of *We* and film thickness

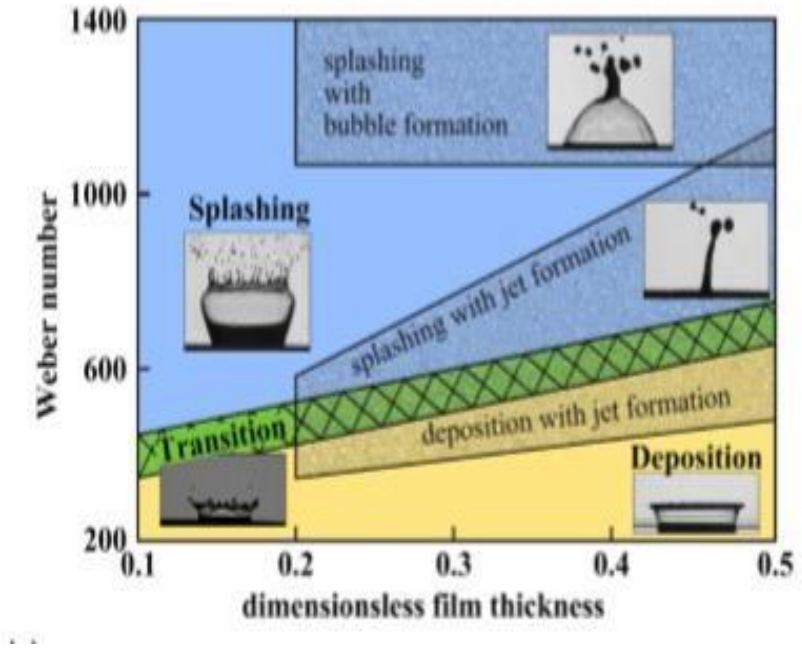

Figure 14: Impact regime for hexadecane one component interaction (Geppert *et al.*, 2017)

Geppert *et al.* (2017), also studied the two-component interaction and concluded that when the non-dimensional film thickness was less than 0.01, holes were observed in the crown wall. This was also observed by Thorddsen *et al.* (2006). Other observations occurring for non-dimensional film thickness less than 0.01 were crown wall break up from the base and a change in the crown wall inclination with the increasing film thickness, which were spotted by Geppert *et al.* (2017) in his studies. This is illustrated in the following figure 15.

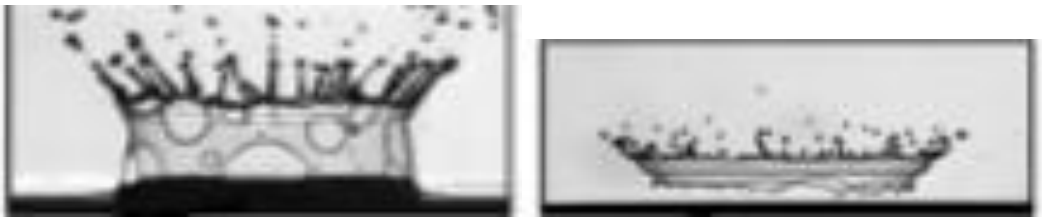

(a) (b)

Figure 15: (a) Hole formation in the crown wall, (b) Crown wall break up from the base (Geppert *et al.*, 2017)

2.3.4 Sommerfeld or Non-dimensional parameter K

The non-dimensional parameter K gives us the splashing threshold. The main problem that has been encountered after reviewing the studies of different researchers is that, based on different operating/experimental conditions the empirical relation for K changes accordingly. According to the previous studies it is difficult to derive a single correlation between the splashing threshold and the non-dimensional parameters *We, Re, Oh* which will satisfy all the conditions. Hence, more work is necessary in developing correlations that will cover a wide range of experimental conditions.

Following are the few empirical correlations given by different researchers for determining splash threshold. Also, it was reported by many researchers that when the value of K fell below its critical value then deposition occurs, else splashing occurs. (Cossali *et al.*, 1996, Yarin and Weiss, 1995, Rioboo *et al.*, 2003 Deegan *et al.*, 2007)

- $\mathbf{Kc = 2100+5880(h^*)1.44}$
- $\mathbf{K = We \cdot Oh^{-0.4} = (Re \cdot We^2)^{0.4}}$
- $\mathbf{K = We^{0.5}\ Re^{0.25}}$

2.3.5 Drop impact on a pool

Drop impact on a pool is another broad sector of research. There has been a comprehensive work done on the analyzing the crater formed when a droplet hits a pool of liquid by Ray *et al*. (2015) who reported that depending on the conditions of impact either a vortex ring is formed after coalescence or a splash is observed after an impact. They conducted their tests for *We* numbers ranging between 50 and 300 and Froude number from 25 to 600. Another work presented by Guilizzoni *et al*. (2019) applied computational fluid dynamics to a study of synchronized multiple droplet impact into a deep pool using the VOF method and validated the results experimentally with high-speed imaging videos. The findings of this work concentrated mainly on the energy conversion between kinetic and surface energy and characterization of the crater formed, depending upon whether it is a single droplet impact or a multiple droplet impact. The crater shape and depth were found to be influenced by surface tension and interspace between the droplets, to a large extent. With the help of numerical simulations along with experimental testing for double and single droplet impact on a deep pool they established that the results for single droplet impact cannot be directly extrapolated for multiple droplet impact to best suit the real-life applications like IC engines, pesticide deposition in agriculture, rain effects on aircraft, wind turbines, etc.

Orozco (2015), reported a study of droplet impact on liquid pool of the same liquid. In this work he used high-speed imaging and VOF method to investigate the effect of liquid properties on instabilities causing Rayleigh jet break-up and consequent secondary atomization. He also developed a regime map to characterize crown formation, crown splash, and Rayleigh jet break-up based on *Oh*. He used a set of fluids to achieve a variation in physical properties and analyzed their effect on break-up mode. Figure 16 (a) and (b) show the regime maps for Rayleigh break up and secondary droplet formation based on Re and *Oh*.

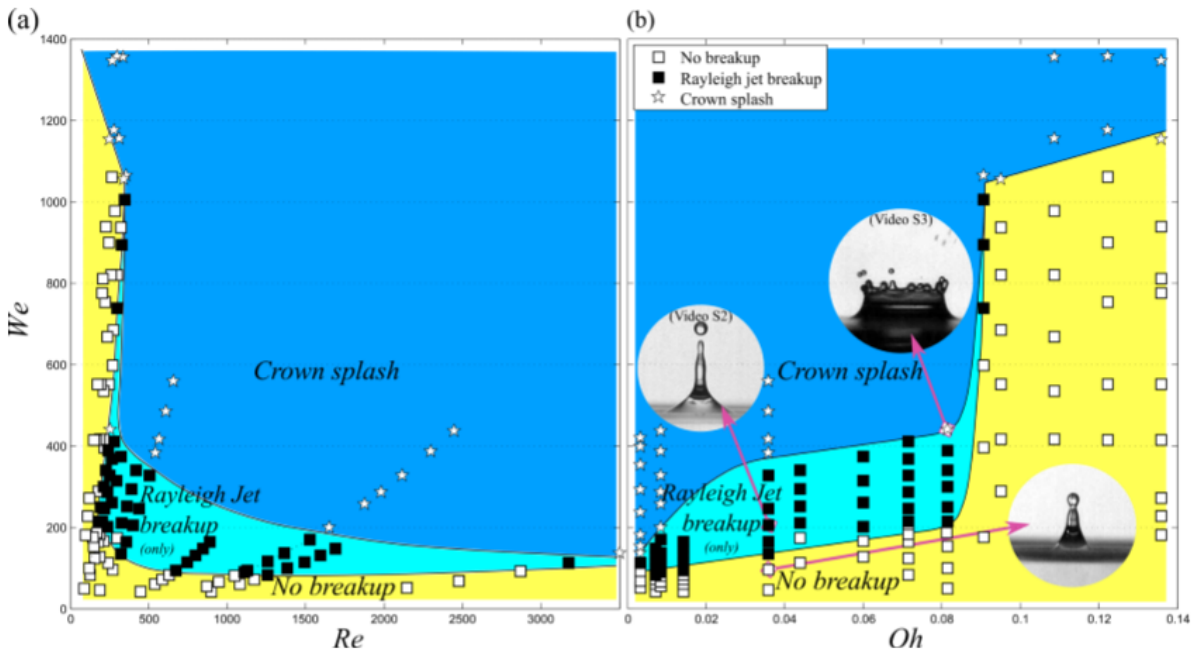

(a) (b)

Figure 16: (a) and (b): Regime maps for Rayleigh jet breakup and subsequent secondary droplets formation based on Re and *Oh* respectively. Filled markers represent the cases where breakup took place and single or multiple secondary droplets were observed. Blank and star symbols represent no breakup and crown splash respectively (Orozco, 2015)

2.4 Inconsistencies in the work done so far

Studies done so far regarding drop impact on a liquid film mainly focus on identifying regimes involved in the drop impact on liquid films and studying their dynamics. Most previously done work has taken liquid films of $0.1 < \delta < 1$ where δ is the non-dimensional film thickness.

Less focus has been given to the drop size distribution and development of probability density functions for the drop size for a large number of varying conditions. Though the abrupt phenomenon occurring in the two component interactions have been identified by Geppert *et al.* (2017) the exact detailed mechanism is not been yet known (Geppert *et al.*, 2017). Another important aspect in the study of drop impact on a liquid film or pool, that is still not researched thoroughly, is characterizing the secondary droplets formed for fluids apart from DI-Water to further develop an understanding of how the fluid properties affect secondary atomization, amount

of fluid or mass of fluid contained in those secondary droplets which is still not much worked on. This is the theme of the research work presented in this thesis dissertation.

2.5 Summary

From this literature review, it can be said that it is essential to examine the drop impact on liquid films with dimensionless film thickness δ <0.1 and > 1 to the limit when film becomes a pool. Also, establishment of *pdf*(d)*s* for fragment size and velocity for each regime considered will help in further advancement of our understanding of drop impact on liquid surface. This in turn will help to optimize the spray in accordance with the application requirements.

3. EXPERIMENTAL SET-UP

The aim of this work is to develop size and velocity *pdfs* for droplets formed due to secondary atomization that happens when a droplet hits a liquid pool of the same liquid. For this Digital Inline Holography (DIH) was used.

3.1 Digital in-line Holography

The Digital in-line Holography experimental set-up used in this work, as shown in Figure 17, was adapted from the set-up of Guildenbecher *et al.* (2017). A laser of 532 nm wavelength and an intensity of up to 300 mW was used as the illumination source. This laser beam is filtered spatially with the help of a ThorLabs Mounted Absorptive Neutral Density Filter, which has specifications as Ø25 mm, Optical Density: 1.0, and SM1-Threaded Mount. The spatially filtered output beam is expanded by a beam expander - ThorLabs Fixed Optical Mount (FMP1 - Fixed Ø1" Optical Mount, 8-32 Tap), and then collimated into a beam using a Malvern biconvex lens having a 600 mm focal length and a 60.3 mm clear aperture. The beam is expanded from 3 to 85 mm by the beam expander and, after collimation by the collimating lens, the beam is directed towards the target droplets. After the beam falls on the target droplets it gets scattered and creates an interference which is recorded using a 20 kHz Photron SA-Z camera.

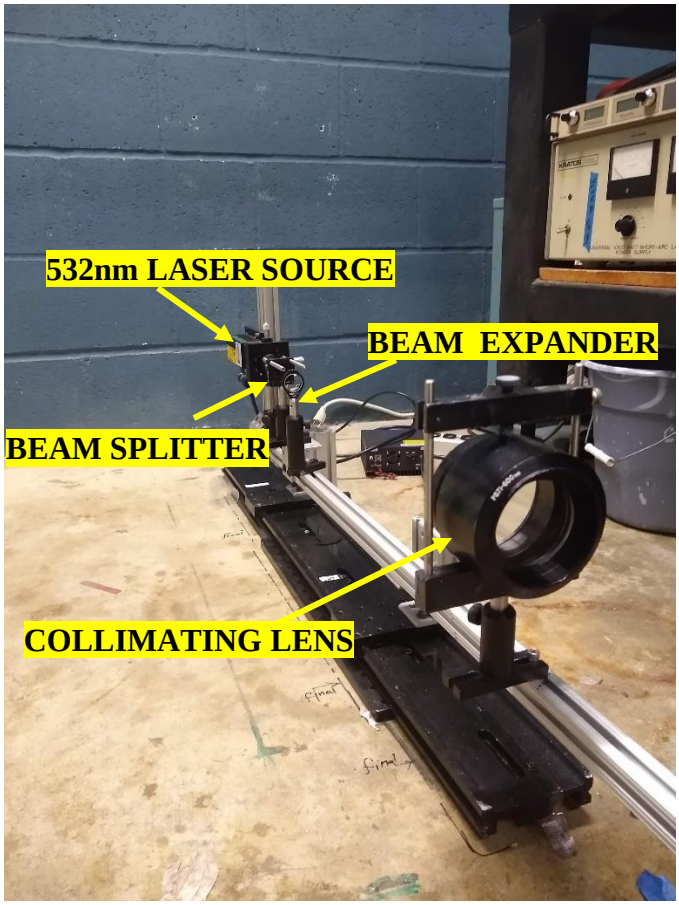

Figure 17: Digital in-line Holography Experimental set-up of optical components

Additionally, a focusing lens, as shown in Figure 18, was used to increase the field of view of the camera. It was placed between the point where actual droplet impacts on the liquid film and the camera. The scattered light from the droplet impact passes through this focusing lens and is directed to the camera. The position of the focusing lens is adjusted along the optical axis in such a way that it lies in a plane slightly offset from the actual focal plane of the lens. This arrangement generates the necessary diffraction pattern which is required to reconstruct holograms of the droplets.

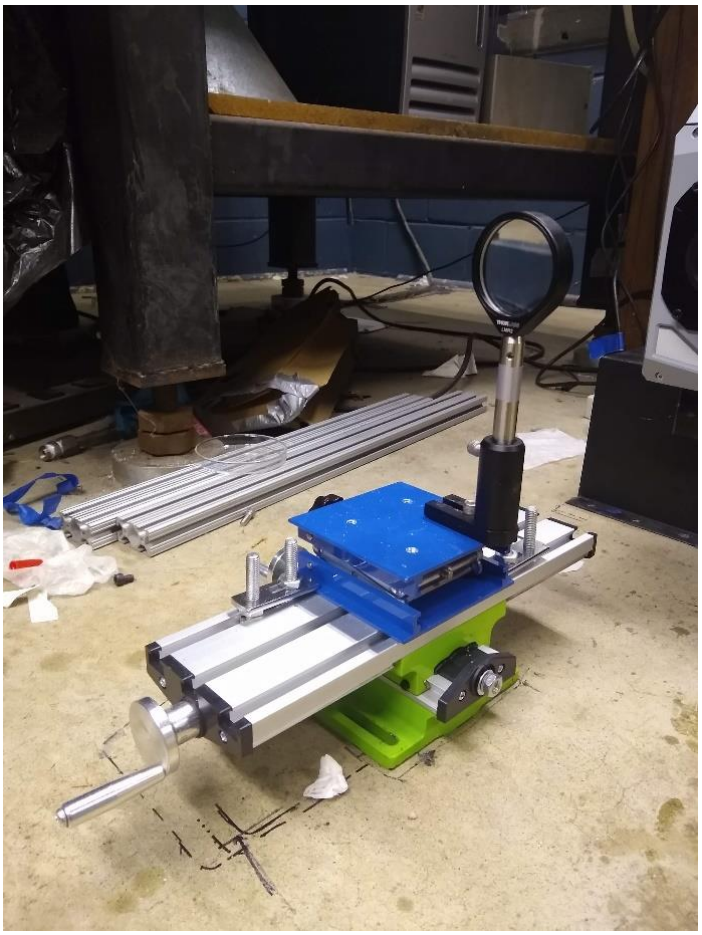

Figure 18: Focusing Lens

3.2 Drop Impact Set-up

To characterize and analyze the effect of drop impact on a pool, a setup consisting of a 75 mm diameter and 17 mm depth glass petri-dish, an 18-gauge syringe and tip, and a New Era Pump Systems, Inc syringe pump is used, as shown in Figure 19. The influence of air draft on the falling drop is avoided by using a plastic tube that stretches over the entire length from the point at which drop falls to the point where the laser interrogation region starts. During every test it is ensured that the drop hits exactly at the center of the petri dish which is filled to the brim. While conducting each test the impacting droplet fluid and the pool fluid is kept similar. For all the tests, the rate of droplet impact is kept constant and equal to 0.2 ml/hr in order to ensure that the pool of liquid remains stationary after a droplet hits it. The diameter of the droplet impacting the pool is 3 mm as adjusted on the syringe pump. The impact droplet size and the uncertainty in the impact droplet diameter is measured from the high-speed images using image acquisition tool.

Figure 19: New Era Pump

3.3 High-speed image acquisition

High-speed images of the droplet hitting the liquid pool are captured using a Photron SA-Z monochrome camera having a 20 µm pixel pitch with a 12-bit ADC depth. The images captured by the camera can be viewed on the computer using the Photron Fastcam Viewer Version 3681 software. All the images were taken at 3000 fps. For DI water, for the case of *We* 1500, exposure time was 1.25 µs whereas for all the other fluids at all the remaining *We* number conditions the exposure time was 0.6 µs. Figure 20 shows Photron SA-Z camera.

Figure 20: Photron SA-Z Camera

3.4 Experimental set-up overview

The droplet injection height is varied to vary the *We* number between 500 and 1500. Three different fluids – DI water, Ethanol, and 77% Glycerol solution were used as the test fluids in order to study the effect of viscosity (*Oh* ranging between 0.0022 to 0.0952) and non-dimensional thickness δ equal to 5.67, on secondary atomization. The petri dish used in the experiment has a diameter of 75 mm and depth of 17 mm. The *We* is varied by varying the height of injection. The height of injection is the distance between the tip of the injection needle and the water surface. Figure 21 illustrates the schematic of the entire experimental apparatus. The focusing lens as shown in figure 18 is placed between the high-speed camera and the target to enhance the field of view.

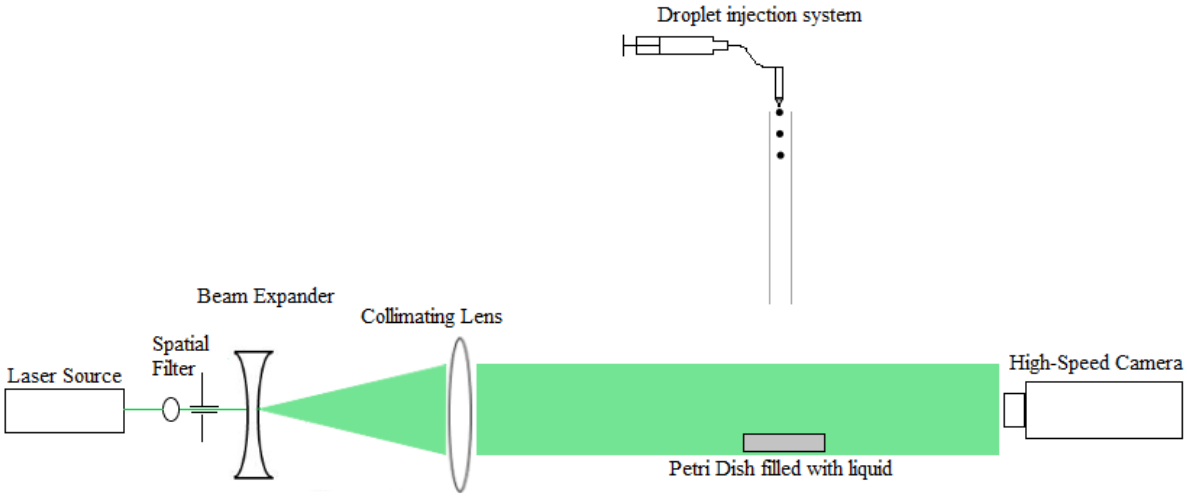

Figure 21: Schematic of the experimental set-up for DIH

3.5 Testing Conditions

3.5.1 Impact height

The characterization of the droplet impacting a pool (non-dimensional thickness: δ = h/d >1 = 5.67) is done by varying the *We* number through variation in the height of injection. Following table illustrates the different test conditions used in this work. Droplets of 3 mm are generated by the droplet generator. Keeping the diameter constant, the impact height is calculated using the physical properties of the fluids and the required *We*.

Table 1: Impact height for different test fluids

***We* (Maximum uncertainty %)**	**Impact height for different fluid (m)**		
	DI Water	**Ethanol 200**	**77 % Glycerol**
530 (5.24 %)	0.65	0.24	0.49
710 (4.19%)	0.87	0.33	0.66
1060 (4.19%)	1.30	0.49	0.99
1500 (4.49%)	1.84	0.69	1.40

3.5.2 Physical properties of the fluids

The fluids with which the testing is performed are chosen in such a way that a wide spectrum of viscosity can covered for studying the influence of changing viscosity on secondary atomization when drop impacts a liquid pool of the same liquid. Table 2 illustrates the physical properties of the fluids tested.

Table 2: Physical properties of the test fluids – DI Water, Ethanol, 77% Glycerol

Fluid	**Dynamic Viscosity μ (Ns/m^2)**	**Surface Tension σ (N/m)**	**Density ρ (kg/m^3)**
DI Water	1.0 e-3 $\pm$ 0.001	0.0053 $\pm$ 0.0001	1000 $\pm$ 25
Ethanol 200	1.2 e-3 $\pm$ 0.001	0.0214 $\pm$ 0.0001	789 $\pm$ 25
77% Glycerol	4.5 e-2 $\pm$ 0.01	0.066 $\pm$ 0.0001	1200 $\pm$ 25

3.6 Uncertainty Analysis

While performing any experiment it is very essential to be aware of the uncertainty prevalent in the entire experiment to know the degree of accuracy of the measurements taken and the results

obtained. This section gives an overview of the uncertainties present in the physical parameters involved in this study – droplet diameter, *We, Oh* based on the work of Kline and McClintock (1953) on uncertainties. The equations used to find the uncertainties are mentioned in this section.

3.6.1 Uncertainty in initial droplet diameter

The desired initial droplet diameter is 3 mm however, the diameter of the initial droplet at the time just before the impact tends to deviate from its true diameter. This happens because the droplet is injected from a height and even if it experiences a downfall in an enclosed chamber there exists a little air drag in the region right before it hits the liquid surface. The presence of air drag causes a very small deformation of the previously spherical droplet and the ratio of semi-major to semi-minor axis of the initial droplet is observed to be in the range of 1 to 1.2. The maximum percent uncertainty diameter observed amongst all *We* is 4.5%.

3.6.2 Uncertainty in *We*

The following equations based on the uncertainty theory presented by Kline and McClintock (1953) are used to find the uncertainty in the *We* (Uwe)

$$Uwe = \left[\left(\frac{\rho}{We}\frac{\partial We}{\partial \rho}U\right)^{\rho^2} + \left(\frac{V}{We}\frac{\partial We}{\partial v}U_v\right)^2 + \left(\frac{d}{We}\frac{\partial We}{\partial d}U_d\right)^2 + \left(\frac{\sigma}{We}\frac{\partial We}{\partial \sigma}\,\mathrm{U}_\sigma\right)^2 \right]^{\frac{1}{2}} \quad (1)$$

Where,

$$\frac{\partial We}{\partial \rho} = \frac{V^2 d}{\sigma} \quad (2)$$

$$\frac{\partial We}{\partial V} = \frac{2\rho V d}{\sigma} \quad (3)$$

$$\frac{\partial We}{\partial d} = \frac{\rho V^2}{\sigma} \quad (4)$$

$$\frac{\partial We}{\partial \sigma} = -\frac{\rho V^2 d}{\sigma^2} \quad (5)$$

Using equation (1) to (5) and performing appropriate calculations the uncertainty in *We* is found to be 5.2 %.

3.6.3 Uncertainty in *Oh*

Like in section 3.5.2, the uncertainty in *Oh* (U_{Oh}) is determined by the following equations based on the uncertainty theory presented by Kline and McClintock (1953).

$$U_{Oh} = \left[\left(\frac{\mu}{Oh}\frac{\partial Oh}{\partial \mu}U_\mu\right)^2 + \left(\frac{\rho}{Oh}\frac{\partial Oh}{\partial \rho}\,U_\rho\right)^2 + \left(\frac{\sigma}{Oh}\frac{\partial Oh}{\partial \sigma}\,U_\sigma\right)^2 + \left(\frac{d}{Oh}\frac{\partial Oh}{\partial d}\,U_d\right)^2\right]^{\frac{1}{2}} \quad (6)$$

Where,

$$\frac{\partial Oh}{\partial \mu} = \frac{1}{\sqrt{\rho\sigma d}} \quad (7)$$

$$\frac{\partial Oh}{\partial \rho} = \frac{\mu}{2\sqrt{\rho^3\sigma d}} \quad (8)$$

$$\frac{\partial Oh}{\partial \sigma} = \frac{-\mu}{2\sqrt{\rho\sigma^3 d}} \quad (9)$$

$$\frac{\partial Oh}{\partial d} = \frac{-\mu}{2\sqrt{\rho\sigma d^3}} (10)$$

Using equations (6) to (10) and performing the appropriate calculations the uncertainty in *Oh* is found to be 3.3%.

3.7 Data collection and limitation of the Matlab Code

The high-speed images (20 droplet samples for each *We*) recorded by the high-speed camera are recorded in a computer and then numerically reconstructed in Matlab to develop holograms. The corresponding Matlab files are used to develop size-number, size-volume and velocity *pdfs*. This is done using a Matlab code. However, there exists a limitation to the code. It sometimes gives error in calling the input Matlab files to generate the *pdfs* and hence, in a few cases the sample size for the *pdfs* is slightly less than the desired sample size of 20 droplets.

4. RESULTS

Digital Inline Holography is used in this work to analyze the behavior when a liquid droplet impacts a liquid pool. After numerically reconstructing the holograms size-number, size-volume, and size-velocity *pdfs* are developed and are illustrated in the following sections. An overview of the event of impact of droplet on the pool surface for three different fluids – DI-Water (deionized water), Ethanol, and 77% Glycerol and the physical interpretation for the event is explained.

4.1 Effect of Ohnesorge number on the crown formation and secondary atomization

Droplet impact on a liquid pool or film is most prominently governed by the parameters of the droplet and the film/pool size, droplet liquid physical properties, droplet impact velocity and the liquid film/pool thickness (Sang Hyuk Lee et al, 2011). Hence, the effect of these parameters on the behavior of the fluid post droplet impact can be incorporated using non-dimensional quantities like Ohnesorge number (*Oh*) and Weber number (*We*). This work comprises of experiments conducted for *We* 530, 710, 1060, 1500, and for three different *Oh* 0.0022 (DI-Water), 0.0053(Ethanol), and 0.0952 (77% Glycerol).

Oh is the ratio of viscosity to the inertial force multiplied by the surface tension. Thus, with an increase in the viscosity, the *Oh* increases and that influences the crown development after the droplet hits the liquid pool.

Consequently, we see a difference in the crown development for DI-water, Ethanol and 77 % Glycerol. The tendency of prompt splash, which is very significant for DI-water at all four *We* numbers – 530, 710, 1060, 1500 and for Ethanol at *We* 1060 and 1500, is not observed for any of the *We* numbers in case of 77% Glycerol. Observing the high-speed images taken for all the three fluids at all the four *We* numbers, it can be inferred that as the viscosity increases, *Oh* increases and it affects the crown height, crown diameter, the plausibility of prompt splash, and the development of the peregrine sheet. With an increase in the droplet and pool liquid viscosity the viscous forces become dominant over the inertial forces which reduces the likelihood of the secondary atomization. It also affects the central jet. The jet height reduces with increased viscosity.

A change in the behavior of the central jet while collapsing is also observed as the viscosity increases.

Following figures 22 through 24 illustrate the change in the crown growth with the change in fluid viscosity for a constant *We* number of 1500:

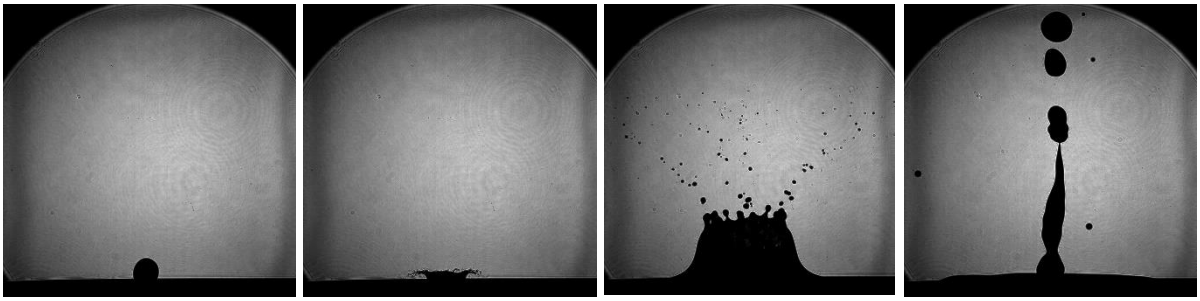

(a) (b) (c) (d)

Figure 22: DI-water droplet impact on DI-water pool at *We* = 1500, *Oh* = 0.0022, (a) Instant of droplet hitting the pool, (b) Prompt splash, (c) Developed crown with peregrine sheet shedding off secondary droplets due to rim instability, (d) Central jet

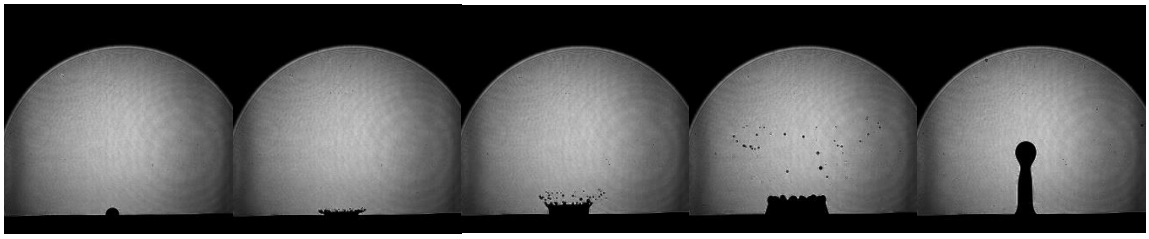

(a) (b) (c) (d) (e)

Figure 23: Ethanol droplet impact on ethanol pool at *We* = 1500, *Oh* = 0.053 (a) Instant of droplet hitting the pool, (b) Delayed splash from ejecta sheet, (c) Jetting phase, (d) Developed crown with peregrine sheet shedding off secondary droplets due to rim instability, (e) Central jet

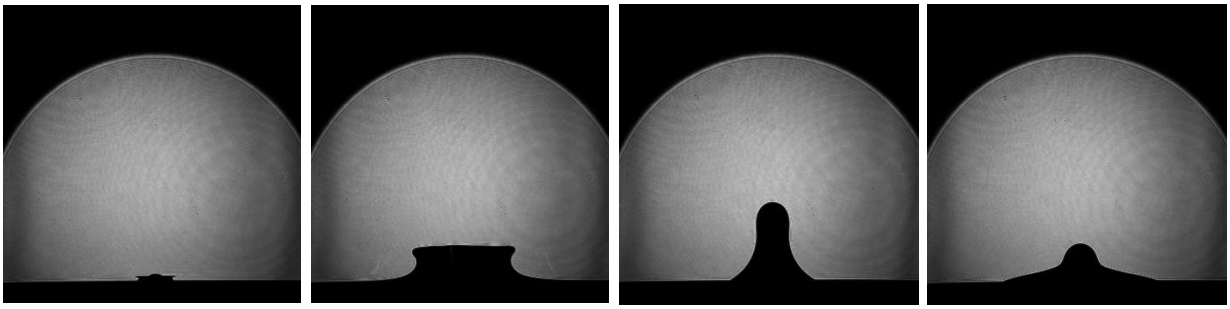

(a) (b) (c) (d)

Figure 24: 77% Glycerol droplet impact on 77% Glycerol pool at *We* =1500, *Oh* = 2.0095 (a) Instant of droplet hitting the pool, (b) Prompt splash, (c) Developed crown with peregrine sheet shedding off secondary droplets due to rim instability, (d) Central jet

As shown for a constant *We* of 1500, as the viscosity increases the height of the fully developed crown decreases. This happens because the increasing viscous forces overcome the available impact energy. With the increasing viscosity the tendency of prompt splash also decreases. The delayed prompt splash is due to the lack of impact momentum against the opposing viscous forces. Hence, at the same *We* 1500, we observe a prompt splash for DI-water, its viscosity being the lowest of the three test fluids, a delayed prompt splash in case of Ethanol, and finally no prompt splash for 77% Glycerol which has the highest viscosity of all the three test fluids. The increased *Oh* also restricts the formation of the peregrine sheet and the secondary atomization from its rim. At the same time, the central jet height is also observed to decrease with the increasing viscosity because both viscous and gravitational forces play a dominant role over the impact momentum which causes the central jet to rise to a maximum height and then collapse under the action of gravitational force.

4.2 Size - number and Size - volume *pdfs*

4.2.1 Size number *pdfs* for DI-water

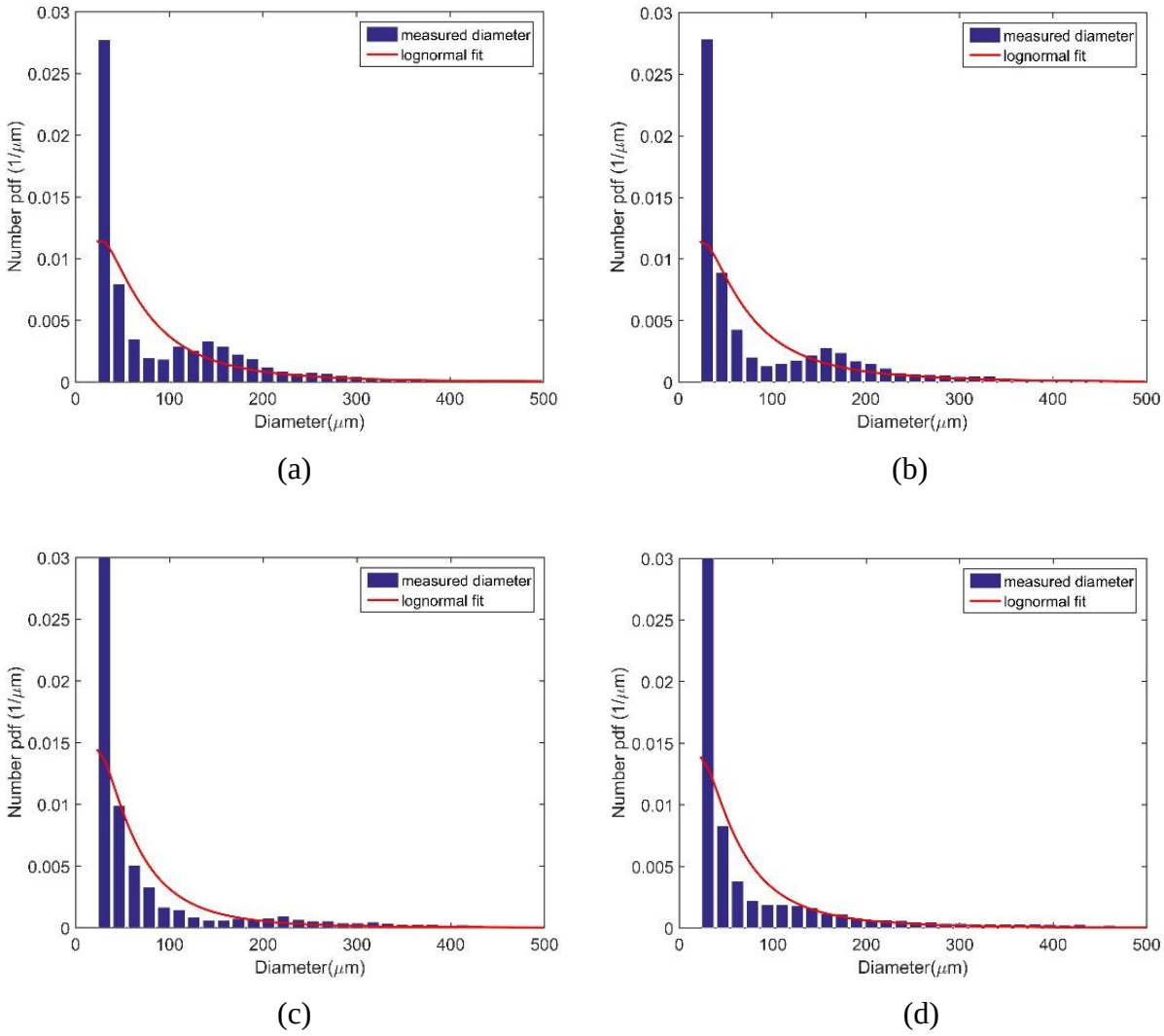

Figure 25: Size-number *pdfs* for DI-water; (a) *We* 530, (b) *We* 710, (c) *We* 1060, (d) *We* 1500

In this work, Digital Inline Holography is used to measure the drop impact fragment sizes and velocities. The figure 25 shows the size-number *pdf* for DI-Water, for four different *We*. The entire experiment is performed for a *We* 530 < *We* < 1500.

It can be seen from figure 25, size-number *pdfs*, that at lower and intermediate *We* a bimodal distribution is obtained. The two peaks *We* occur at 25 to 50 µm while a maximum of the remaining secondary droplets have sizes around 150 µm. At *We* 1060 we see a single peak at 25 to 50 µm droplet diameter. However, a small secondary peak exists at around 200 to 300 µm. At *We* 1500, there is clearly only a single peak occurring at 25 to 50 µm. This means that at very high *We* the majority of secondary droplets formed are of smaller size and a small percentage of droplets are larger. With the increasing *We*, the probability of obtaining secondary droplets of size range 25 µm to 50 µm, increases. These secondary droplets are 0.0083 to 0.0166 times the initial droplet diameter. The shift from bimodal to unimodal distribution with increasing *We* can be attributed to the increasing impact velocity. The secondary atomization at higher *We* is more pronounced as the aerodynamic forces overcome the viscous and surface tension forces. This results into a higher number of smaller size secondary droplets at higher *We*.

4.2.2 Size volume *pdfs for* DI-water

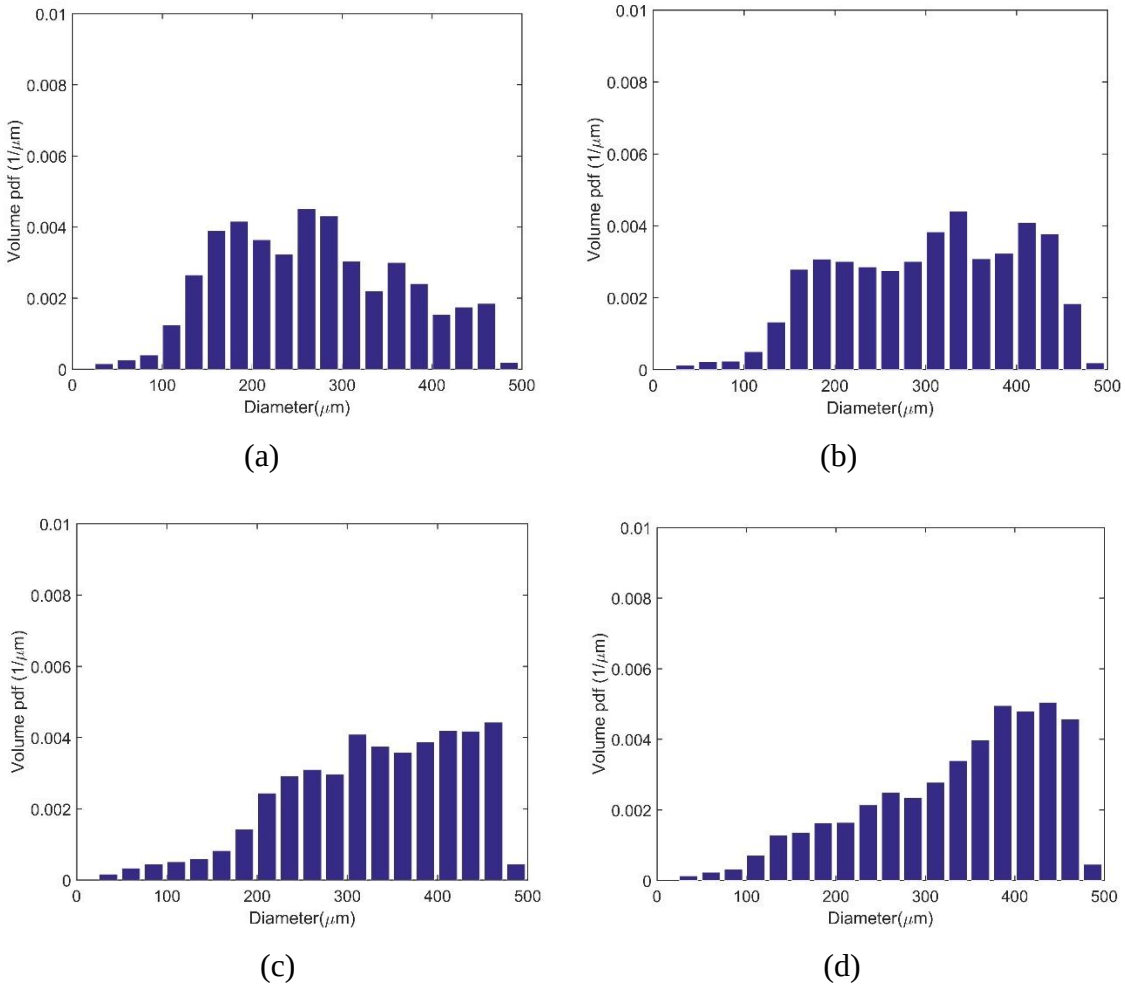

Figure 26: Size-volume *pdfs* for DI-Water; (a) *We* 530, (b) *We* 710, (c) *We* 1060, (d) *We* 1500

The figure 26 presents the size-volume *pdfs* for droplet impact on a liquid pool with the droplet and the pool liquid being DI-Water. At *We* 530, a trimodal distribution occurs with the three peaks occurring for a diameter range of 180 to 200 µm, a diameter range of 280 to 300 µm, and at 350 to 400 µm. At *We* 710 the distribution again, shows three peaks at around 200 µm, at 350 µm, and at around 450 µm. At *We* 1060, the *pdf* rises steeply and then remains fairly constant over a diameter range of 300 to 500 µm. Finally, at *We* 1500, peak can be seen after a gradual rise at around 400 µm to 500 µm. Thus, as *We* increases the distribution tends to become unimodal from trimodal, with low *We* showing three peaks and the high *We* showing a single peak. The

intermediate *We* show a flat distribution over a wide range of droplet diameters. This trend of three peaks being observed from the distributions at *We* 530 and 710, as mentioned above, may be because of the different size droplets occurring at the different stages of the crown evolution. Small sized droplets generated by the ejecta sheet correspond to the first peak, medium sized droplets come from the rim of the peregrine sheet due to rim instability, and the large sized droplets come from pinching off from jets formed on the rim of the peregrine sheet. This is illustrated by the figure 27 through figure 30 below.

For *We* 530 and *We* 710, the ejecta sheet sheds off a number of secondary droplets. This is known as prompt splash and is responsible for very small size droplets that occur at the initial time of impact or during the primary phase of the crown formation. As the time proceeds, the crown increases in size by forming a peregrine sheet. The rim of this sheet sheds off medium and large size droplets. This happens by virtue of the rim instability that occurs accompanied by the initial instability contributed by the ejecta sheet which gives rise to the jet formation on the rim. As *We* increases the intensity of the initial instability increases. Thus, at higher *We* the jets are formed earlier on the crown rim than at lower *We*. Secondary droplets pinch off from these jets formed on the rim.

An additional observation is that the peak value increases with increasing *We*. This happens as a result of increasing impact energy with increasing impact velocity. At low *We*, the impact momentum is low and hence the viscous and surface tension forces stay dominant over the aerodynamic forces. This causes less fluid to be displaced from the pool and a smaller number of secondary atomized droplets. Conversely, at higher *We* the impact energy is high and that leads to more liquid being displaced along with a larger number of smaller size secondary droplets. The intermediate *We* case, where a flat section of *pdf* is observed, is a transition zone between the lower and higher *We* cases. The impact energy also being in between that at lower and higher *We* so the amount of fluid displaced is between that displaced for the lower and higher *We* cases.

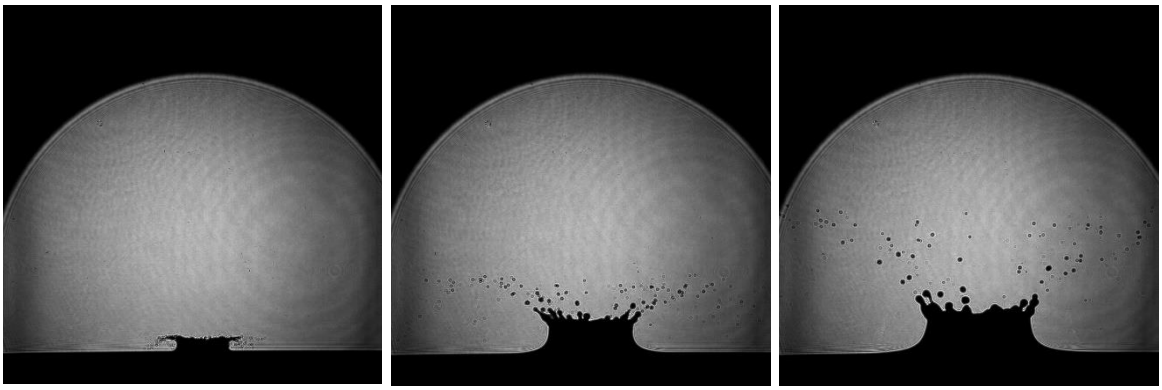

(a) t = 20.9856 s (b) t = 20.9883 s (c) t = 20.9916 s

Figure 27: Crown evolution over time at *We* 530 for DI-Water. (a) Ejecta sheet generating small secondary droplets, (b) Developing peregrine sheet generating medium sized droplets, (c) Developed peregrine sheet generating large sized droplets

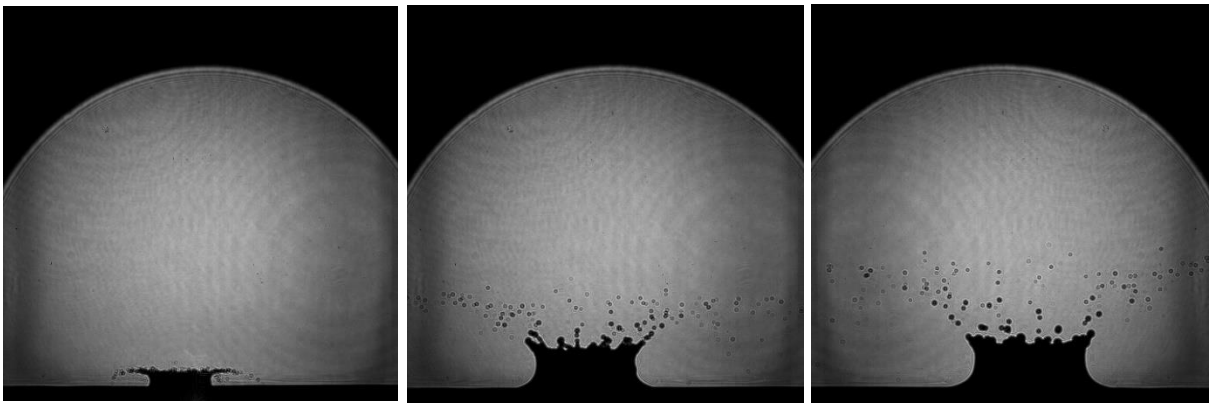

(a) t = 8.7106 s (b) t = 8.7133 s (c) t = 8.7146 s

Figure 28: Crown evolution over time at *We* 710 for DI-Water. (a) Ejecta sheet generating small secondary droplets, (b) Developing peregrine sheet generating medium sized droplets, (c) Developed peregrine sheet generating large sized droplets

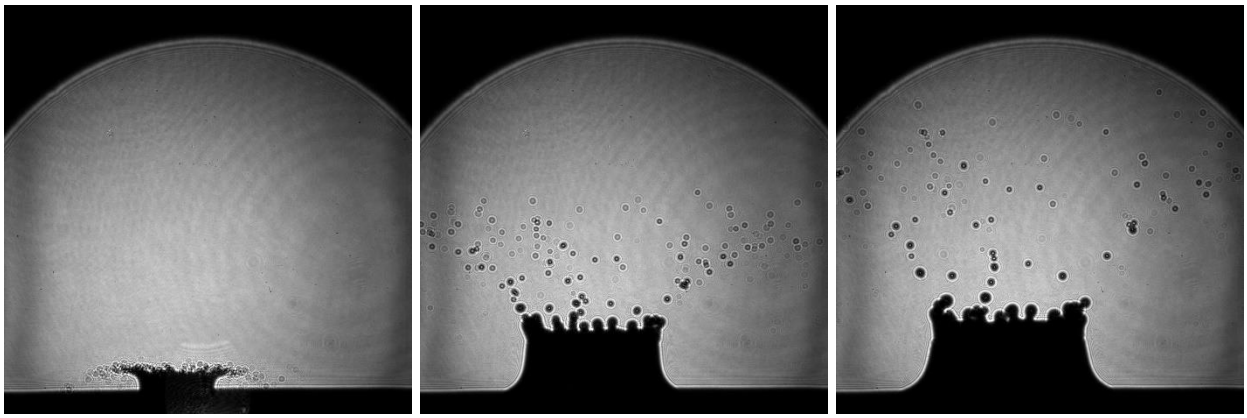

(a) t = 24.6803 s (b) t = 24.6843 s (c) t = 24.6870 s

Figure 29: Crown evolution over time at *We* 1060 for DI-Water. (a) Ejecta sheet generating small secondary droplets, (b) Developing peregrine sheet generating medium sized droplets, (c) Developed peregrine sheet generating large sized droplets

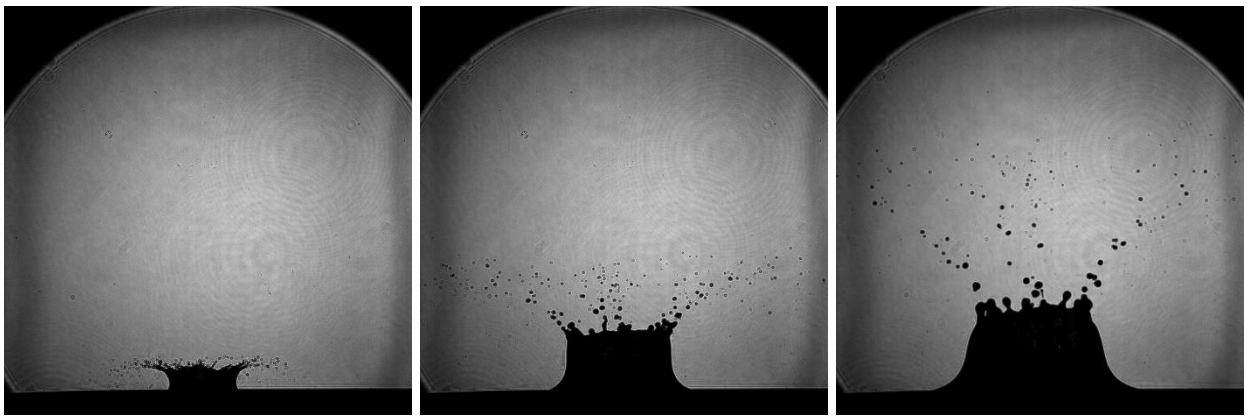

(a) t = 4.2763 s (b) t = 4.2780 s (c) t = 4.2813 s

Figure 30: Crown evolution over time at *We* 1500 for DI-water. (a) Ejecta sheet generating small secondary droplets, (b) Developing peregrine sheet generating medium sized droplets, (c) Developed peregrine sheet generating large sized droplets

4.2.3 Size-number *pdfs* for Ethanol

Ethanol shows secondary atomization only at *We* 1060 and 1500.

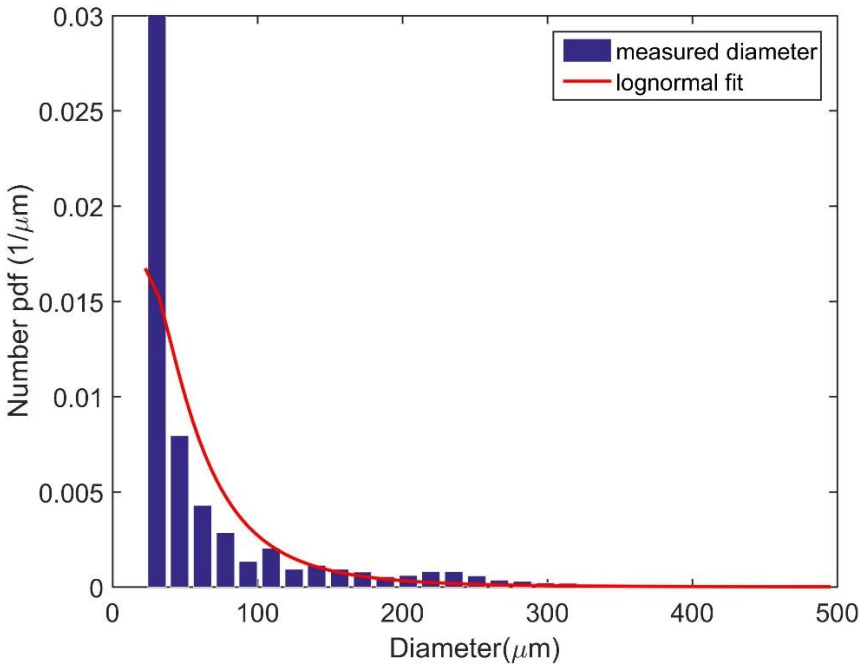

Figure 31: Size-number *pdf* for Ethanol at *We* 1060

At *We* 1060, the distribution is trimodal however, two out of three peak diameters have lower probability, so the distribution is dominated by the first peak at 25 to 50 µm. The second and third peaks can be observed at 110 µm and 250 µm respectively.

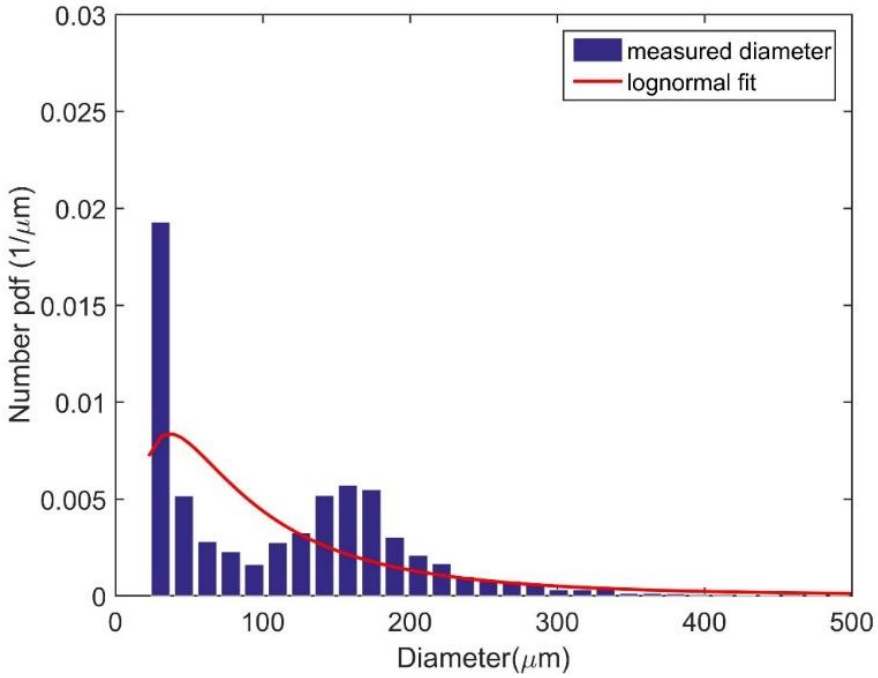

Figure 32: Size-number *pdf* for Ethanol at *We* 1500

The size-number *pdf* for ethanol at *We* 1500 is shown in the figure 32. It can be seen from the figure 32 that the distribution is bimodal, and the two peaks occur at around 25 to 50 µm and 150 µm to 180 µm. It is also clear from that the majority of secondary droplets formed are of size 25 to 50 µm.

From the figures 31 and 32 it can be seen that the probability of getting smaller secondary droplets is higher at *We* 1060 than *We* 1500 which contradicts the observation that as *We* increases, the impact energy increases which gives better secondary atomization. However, in the case of Ethanol, as can be seen from the high-speed videos of the actual droplet impact, secondary atomization happens at *We* 1060 only due to prompt splash whereas at *We* 1500 it occurs due to both prompt splash and jetting from the rim of the peregrine sheet. The secondary atomization that happens because of pinching off from the jets at the rim of the crown usually gives large sized droplets as compared to those obtained from the prompt splash. Hence, the maximum peak is higher in case of *We* 1060 than for *We* 1500 for Ethanol 200.

4.2.4 Size-volume *pdfs* – Ethanol

The size-volume *pdf* for Ethanol at *We* 1060 indicates that most of the secondary droplet volume is contributed by droplets in the size range of 200 to 300 µm. The distribution has three peaks the first at the droplet diameter of 180 µm, second and highest peak at around 250 µm, and the third peak at around 450 µm. Secondary atomization at *We* 1060 for Ethanol takes place because of prompt splash only and hence, the third peak observed in the distribution can be said to have occurred because of the uncertainty in the DIH post processing code capability.

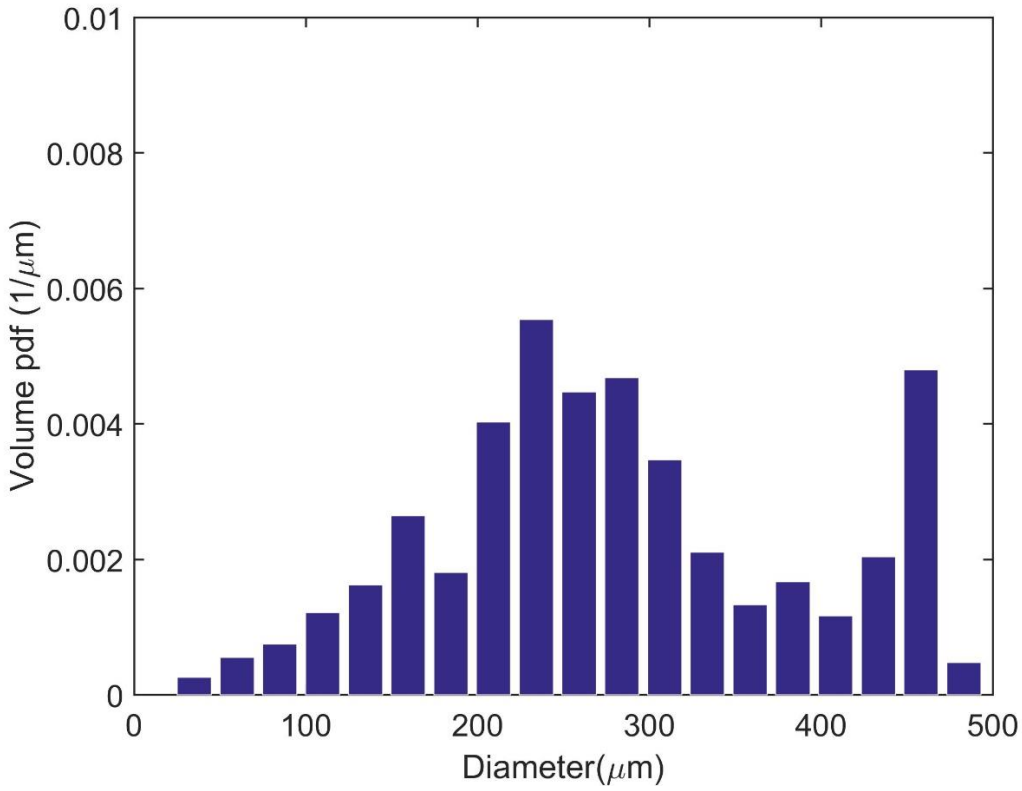

Figure 33: Size-volume *pdf* for Ethanol at *We* 1060

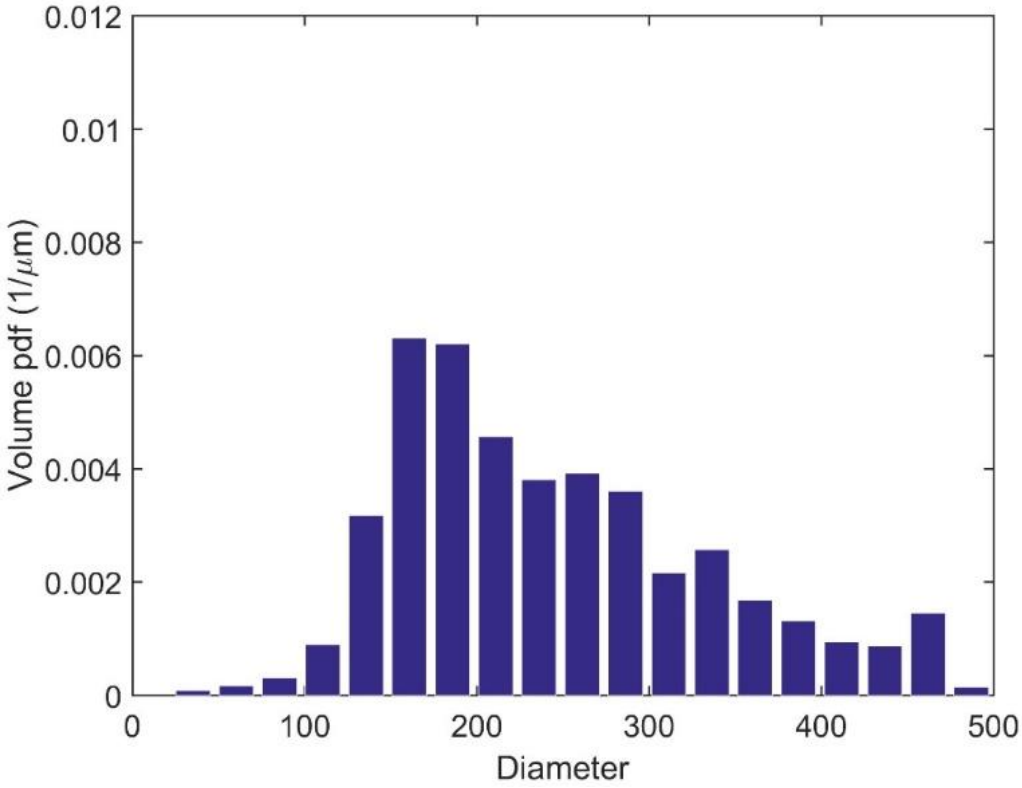

Figure 34: Size-volume *pdf* for Ethanol at *We* 1500

The size-volume *pdf* for Ethanol is shown above for the case of *We* 1500. The distribution is trimodal with the three peaks occurring at around 180, 250 and, 330 µm. The maximum contribution towards the total volume of secondary droplets is from the secondary droplets having a size around 180 µm. These large sized secondary droplets are formed due to crown splash occurring at *We* 1500. Also, the lower surface tension of ethanol promotes earlier jet formation on the crown rim which disintegrate into larger secondary droplets.

4.3 Velocity *pdfs*

The velocity *pdfs* have been developed at all *We* and for all the fluids showing secondary atomization. These velocity *pdfs* indicate the velocity of the secondary droplets that are formed after the initial droplet hits the pool. The velocity *pdfs* are generated for the droplet velocities in x, and y. The direction of initial droplet that is falling vertically downwards is considered as positive

x-direction. The following schematic illustrates the frame of reference considered while developing the velocity *pdfs*.

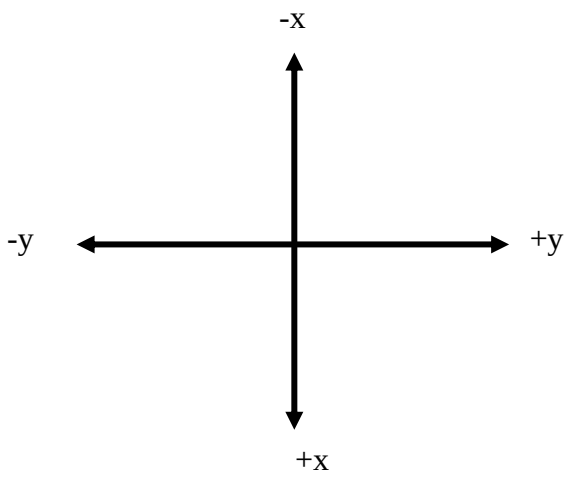

Figure 35: Co-ordinate system of reference

4.3.1 *Vx* velocity *pdfs* for DI-water

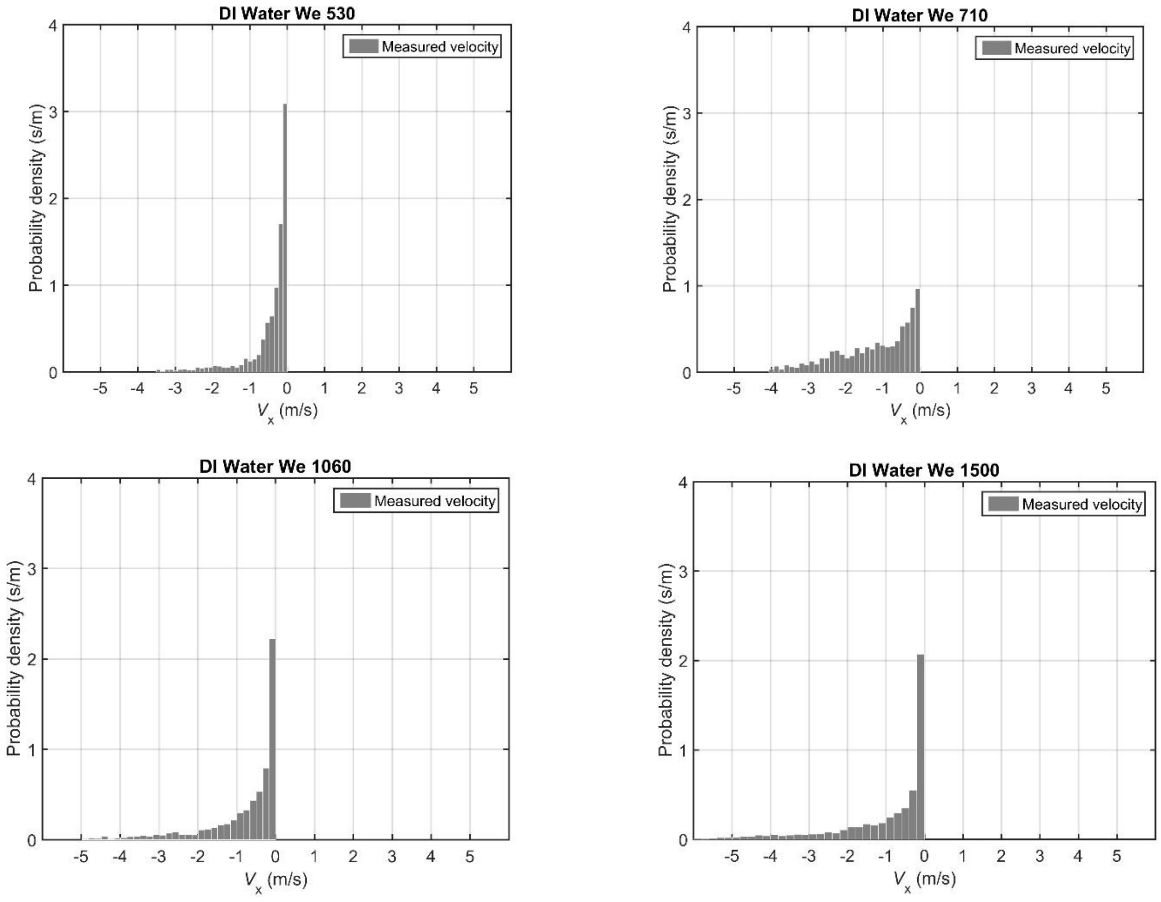

Figure 36: Velocity *pdfs* for *Vx* (velocity of the droplets in x-direction) for DI-Water at *We* 530, *We* 710, *We* 1060, and *We* 1500

The velocity *pdfs* for *Vx* (velocity of secondary droplets in x-direction) have been shown in the above figure 36. As the *We* increases from 530 to 1500, the distribution is observed to be more spread out about zero on the velocity axis. At the same time, with the increasing *We*, the probability of finding the droplets having zero velocity in x-direction is decreasing. This trend can be attributed to the increasing impact energy which causes enhanced secondary atomization and hence gives the secondary droplets enough additional momentum to overcome viscous, surface tension and gravitational forces and accelerate. A sudden drop in the peak at *We* 710 is due to a small sample size.

4.3.2 *Vy* velocity *pdfs* for DI-Water

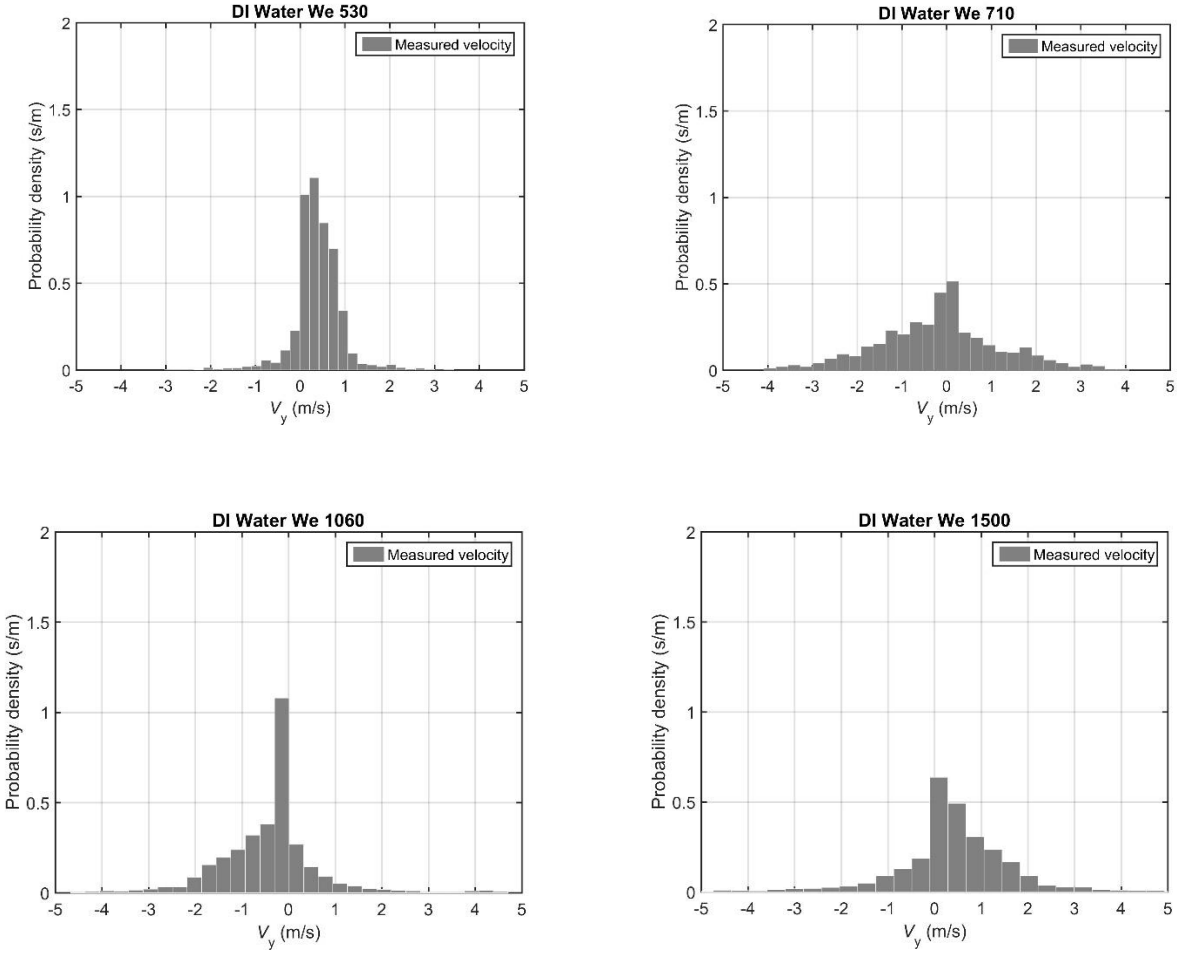

Figure 37: Velocity *pdfs* for *Vy* (velocity of the droplets in y-direction) for DI-Water at *We* 530, *We* 710, *We* 1060, and *We* 1500

The *pdfs* shown above in figure 37 for *Vy* indicate velocity of the secondary droplets in y-direction. The distribution for each *We* is skewed about zero velocity. This is because the secondary droplets spread almost symmetrically about the center of the crown in y-direction. The probability of finding secondary droplets with zero *Vy* velocity tends to decrease with the increasing *We* which results into a more spread out type of distributions as can be seen from the above *pdfs.* At *We* 530, the velocity *pdf* is clustered around zero *Vy* velocity. This indicates that out of all the secondary droplets formed a majority have a zero *Vy* velocity and the remaining have very small *Vy* velocity.

This is because the impact energy at *We* 530 and *We* 710 is less and hence, the momentum necessary for the acceleration of the droplets after overcoming the viscous and surface tension forces is less. However, at *We* 1060, the distribution is spread out as compared to that occurring at *We* 530. This happens due to the greater impact energy at higher *We* which leads to a greater momentum that overcomes the velocity opposing forces – viscous and surface tension forces. Thus, the secondary droplets shed by the crown rim travel with a higher velocity at higher *We* result into a well distributed velocity *pdf.* As the *We* increases further to 1500, the peak of the distribution also reduces to 0.5 from 1 indicating that the probability of finding secondary droplets with non-zero velocity is almost half of what we observe at *We* 1060. This is because of the increased impact energy as explained before. Sudden drop in the peak for *We* 710 and a more spread out distribution than that seen at *We* 1060 is due to a smaller sample size used to generate the respective *pdf*. Smaller sample size was used to resolve an error occurring while running the Matlab code *pdf* generation.

4.3.3 *Vx* velocity *pdfs* for Ethanol

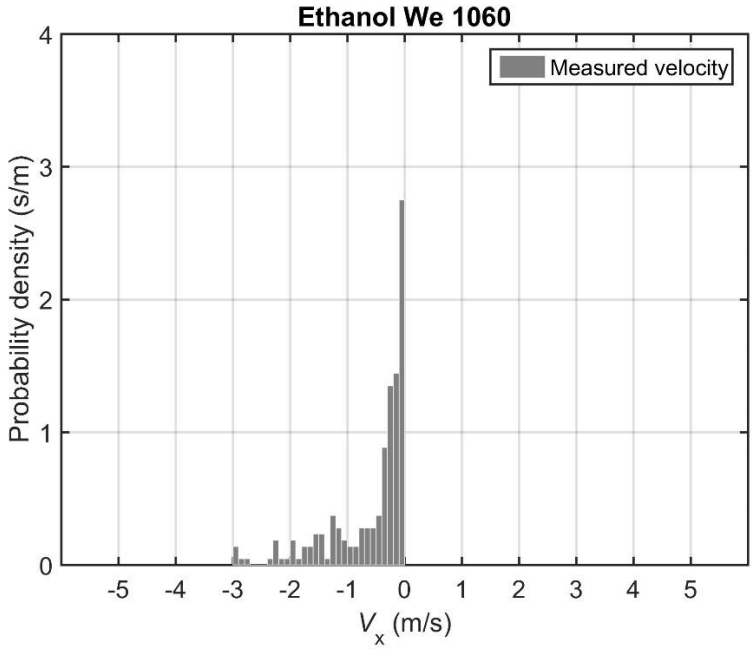

Figure 38: Velocity *pdfs* for *Vx* (velocity of the droplets in x-direction) for Ethanol at *We* 1060

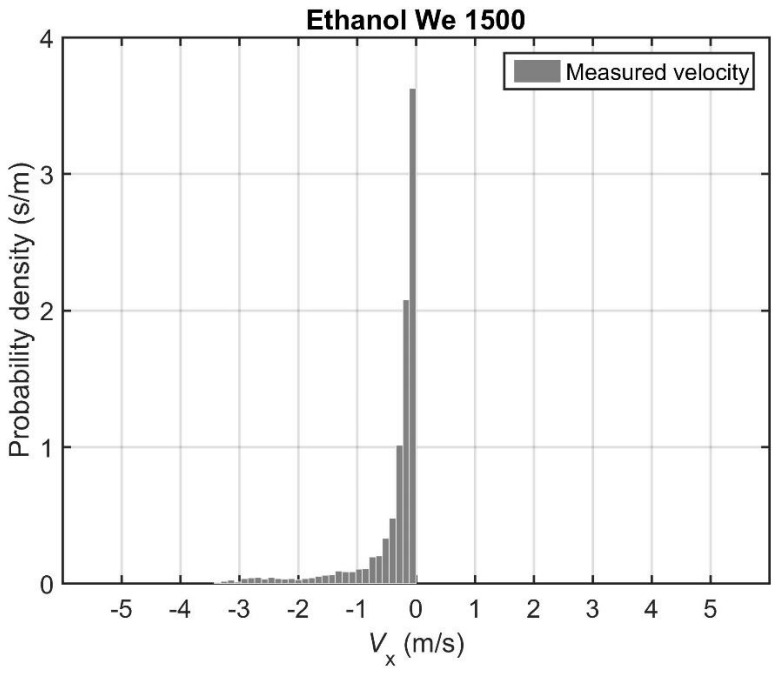

Figure 39: Velocity *pdfs* for *Vx* (velocity of the droplets in x-direction) for Ethanol at *We* 1500

For Ethanol, secondary atomization is observed only at *We* 1060 and 1500 because the impact energy available at *We* 530 and *We* 710 is not sufficient to overcome the surface tension and viscosity which prevents the formation of the secondary droplets.

The *Vx pdf* for both *We* 1060 and *We* 1500 suggests that most of the droplets have almost zero velocity in x-direction. The *Vx pdf* for *We* 1060 however, has a lower peak than that seen in case of *We* 1500. This is because at *We* 1060 all the secondary droplets originate from the prompt splash only, which move in the x-direction as the crown rises. However, in case of *We* 1500 the secondary atomization happens both because of prompt splash and pinching-off from the peregrine sheet rim or crown splash. Thus, the distribution peak shifts to a higher level because the droplets originating from the peregrine sheet rim have almost zero velocity in the x-direction as they spread out mainly in the y-direction.

4.3.4 *Vy* velocity *pdfs* for Ethanol

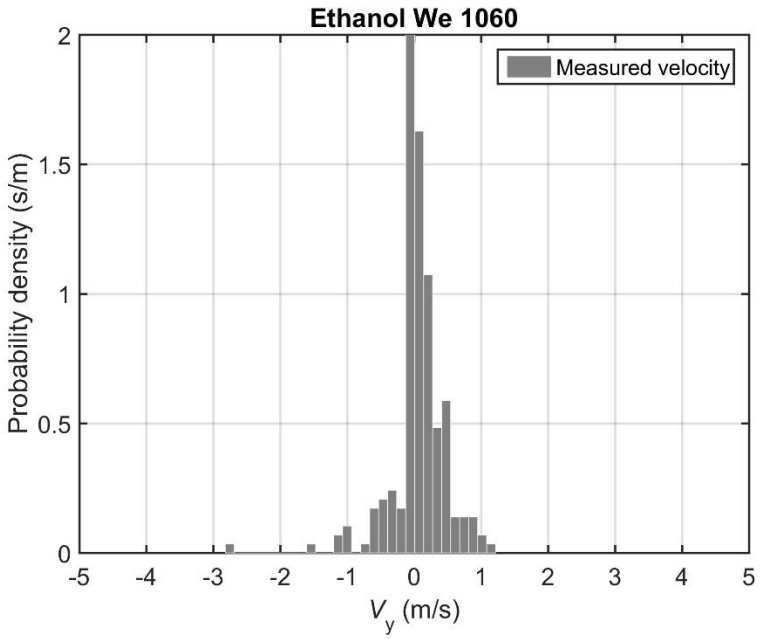

Figure 40: Velocity *pdfs* for *Vy* (velocity of the droplets in y-direction) for Ethanol at *We* 1060

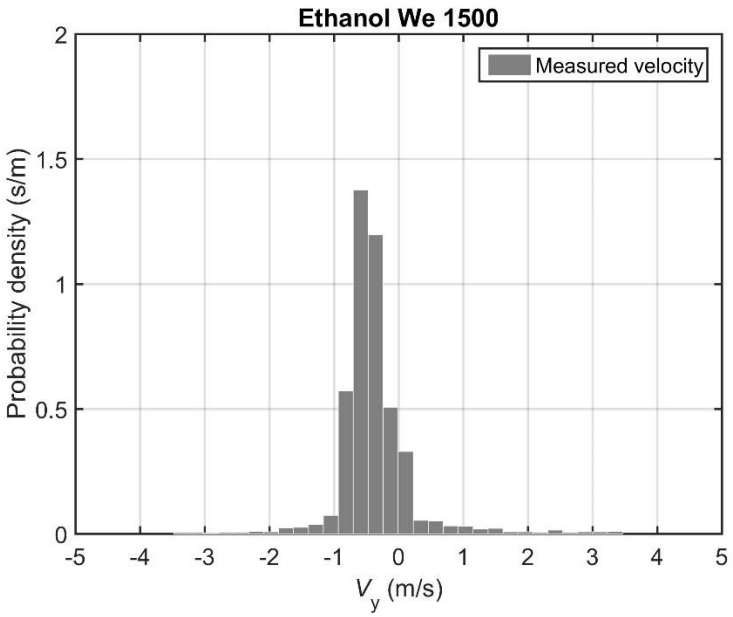

Figure 41: Velocity *pdfs* for *Vy* (velocity of the droplets in y-direction) for Ethanol at *We* 1500

The *Vy pdf*, shown in figure 41, shows a skew symmetric distribution about zero which suggests that the secondary droplets formed from the crown move with equal velocity in +y and -y direction. The peak of the distribution is higher for *We* 1060 than for *We* 1500 because impact momentum increases, and the disruptive forces dominate the surface tension and the viscous forces. Due to the same reason a greater number of secondary droplets have non-zero y-velocity which is why the distribution is smoother about its peak for *We* 1500 than *We* 1060 as the number of secondary droplets having a small yet non-zero velocity increases.

5. SUMMARY AND CONCLUSIONS

This study is focuses on the behavior of three different fluids in case of the droplet impact of the fluid on the surface of the liquid pool using DIH. Images of this event are captured using a high-speed camera, then numerically reconstructed using Matlab for extracting useful information. Information regarding the secondary droplets obtained after post-processing is used to develop size – number, size – volume and velocity *pdfs* for each fluid under different test conditions. Three fluids are tested, each at four different *We* numbers which covers a broad range of *We* number from 530 to 1500. Not only the effect of *We* but also the effect of *Oh*, ranging between 0.0022 to 0.0952, on the droplet impact on a liquid pool is studied in this work. All the experiments are conducted at a constant non-dimensional thickness of 5.67. Both qualitative and quantitative inferences about the behavior are drawn based on the available high-speed images and the generated *pdfs*.

Firstly, the effect of *Oh* is illustrated in the results section. At a constant *We* with increasing *Oh,* from 0.0022 to 0.0952, the probability of secondary atomization decreases. Secondary atomization is only observed for DI-Water at all four test conditions (*We* = 530, *We* = 710, *We* = 1060, *We* = 1500) and for Ethanol at higher *We* numbers (*We* = 1060 and *We* = 1500). It is not observed for 77% Glycerol at any of the four *We* numbers. Increased *Oh* decreases the maximum height the central jet can achieve.

The size-number *pdfs* for DI-Water are generated at all four *We*. The *pdfs* illustrate that as the *We* increases the probability of getting secondary droplets of the size 25 µm - 50 µm increases with a very few secondary droplets of size 150 µm at low *We* 530 and *We* 710. These droplets originate from the prompt splash and the jetting from the rim of the peregrine sheet due to the rim instability known as crown splashing. The *pdf* also shifts from multi-modal to unimodal with increasing, *We*. In case of ethanol, as secondary atomization is observed only at *We* 1060 and *We* 1500, size-number *pdfs* are generated only for those two cases. From those size *pdfs* it is inferred that as *We* increases the tendency of crown splashing increases. At lower *We* for ethanol, there is no secondary atomization and it is first observed at *We* 1060 where it happens only because of prompt splashing. At *We* 1500 the secondary atomization happens because of both prompt and crown splashing. As

seen from the high-speed videos, prompt splashing gives smaller diameter droplets (25 µm – 50 µm) whereas crown splashing gives larger size secondary droplets (150 µm) relative to the prompt splashing. Hence, the secondary droplets size number *pdf* in case of *We* 1060 has a maxima at 25 µm – 50 µm and two peaks at 25 µm – 50 µm and 150 µm – 180 µm for *We* 1500.

The size-volume *pdfs* are also generated at all four *We* for DI-Water. As the *We* increases, the peak shifts towards larger drop diameters because at higher *We* more fluid is displaced from the pool. Increased impact energy contributes to early jetting from the crown rim which gives few, yet relatively larger, droplets that mainly contribute to the majority of the secondary droplets' volume.

Velocity *pdfs* are also generated for DI-Water at all four *We* in the horizontal and vertical directions. The distribution for vertical velocity for DI-Water at all *We* indicates that a majority of the secondary droplets have almost zero velocity in x-direction. However, as the *We* increases, the probability of getting a zero *Vx* velocity decreases. Similarly, in case of the distributions for *Vy* for DI-Water, the peak value or the probability of getting zero velocity decreases with the increasing *We*. The distribution for *Vy* is symmetric as the crown is symmetric about x-axis. Increased impact energy gives a more uniform *Vy* velocity distribution.

The size-number and size-volume *pdfs* generated for ethanol for *We* 1060 and *We* 1500. High-speed video of the actual impact phenomenon suggests that secondary atomization occurs only at *We* 1060 and *We* 1500 and the secondary atomization occurring at *We* 1060 is only by prompt splashing in case of ethanol. However, at *We* 1500 the secondary atomization is a result of prompt and crown splashing as well. It is also observed that a bimodal distribution at a higher *We* of 1500 for ethanol is because secondary atomization occurs because of both prompt and crown splash and the lower surface tension accompanied by higher impact energy, for ethanol, promotes earlier jetting and pinching off of the secondary droplets.

5.1 Future Scope

In the present work, DIH has been used to understand the droplet impact on a pool surface of the same liquid both qualitatively and quantitatively. Based on the collected data, size-number, size-volume and velocity *pdfs* have been developed which further facilitates to understand the droplet impact on the pool surface phenomenon in depth. Studying the *pdfs* we can get a better idea of the dependency of secondary atomization on the non-dimensional parameters, *We* and *Oh* at a constant non dimensional thickness δ of the pool.

There is yet, a lot more to explore in this field and hence, following are a few recommendations for conducting future work in the analysis of droplet impact on liquid pool.

This work is limited to *We* = 1500 due to the infrastructural constraints. Thus, similar experiments as conducted in this work can be conducted at, *We* higher than *We* 1500 to further understand the phenomenon at higher *We*. At the same time, as the current work uses only three test fluids- DI- Water, Ethanol, and 77% Glycerol, future experiments can be conducted, to understand the effect of viscosity on the droplet impact on liquid pool, with fluids like Diesel, Gasoline and, Jet engine fuel which have direct commercial applications.

The current work has all the experiments carried out at ambient pressure and temperature. Future experiments, using DIH, can be conducted under high pressure and temperature conditions to understand the effect of the environmental conditions on secondary atomization. Also, the temperature of the test fluid and the injection pressure of the fluid could also be varied to understand the influence of these physical fluid parameters on the secondary atomization.

In this work, all the study has been conducted for a single non-dimensional thickness δ =5.67 of the liquid pool. This study can be further extended to examining the phenomenon of droplet impact on liquid pool using DIH by varying the non-dimensional thickness of the pool.

REFERENCES

1. Banks, *et al.,* "Effects of drop and film viscosity on drop impacts onto thin films", Atomization and Sprays, Vol. 23, pp. 555-570, 2013

2. Coghe, *et al.,* "Single drop splash on thin film: measurements of crown characteristics" ILASS Europe, 1999.

3. Cossali, *et al.,* "The impact of a single drop on a wetted solid surface", Experiments in Fluids, Vol. 22, pp. 463 – 472, 1997

4. Cossali, *et al.,* "The role of time in single drop splash on thin film", Experiments in Fluids, Vol. 36, pp.888-900, 2004

5. Deegan, *et al.,* "Complexities of splashing", Nonlinearity, IOP Publishing Ltd and London Mathematical Society, Vol. 21, 2007

6. Geppert, *et al*.," A benchmark study for the crown-type splashing dynamics of one- and two-component droplet wall–film interactions", Experiments in Fluids, Vol. 58, 2017

7. Guildenbecher, *et al.*, "Viscous drops impacting thin liquid surfaces: experimental quantification of secondary drop fragment sizes and velocities", ILASS Americas 27th Annual Conference on Liquid Atomization and Spray Systems, 2015

8. Guildenbecher, *et al.*," Digital Inline Holography to quantify secondary droplets from the impact of a single drop on a thin film" Experiments in Fluids, Vol.55, 2014

9. Guilizzoni, *et al.,*" Synchronized Multiple Drop Impacts into a Deep Pool", Fluids, Vol.4, 2019

10. Josserand, *et al.,* “Droplet impact on a thin liquid Collision”, Journal of Fluid Mechanics, Volume 802, pp. 775-805, 2016

11. Josserand *et al*., “Droplet splashing on a thin liquid film”, Physics of Fluids, Vol.15, 2003

12. Kang, “Experimental Study of the Phenomenon of Droplet Impact upon a Liquid Surface”, Journal of Applied Fluid Mechanics, Vol. 9, pp. 757-765, 2016.

13. Katz and Sheng, “Applications of Holography in Fluid Mechanics and Particle Dynamics”, Annual Review of Fluid Mechanics, Vol. 42, pp. 531-555, 2010

14. Kittel, *et al.,* 2017, “Splashing of a very viscous liquid drop impacting onto a solid wall wetted by another liquid”, ILASS–Europe, 2017

15. Lee, *et al.,* “A numerical analysis of drop impact on liquid film by using a level set method”, Journal of Mechanical Science and Technology, Vol.25, pp. 2567-2572, 2011

16. Liang, *et al.,* “Crown behavior and bubble entrainment during a drop impact on a liquid film”, Theoretical and Computational Fluid Dynamics, Vol. 28, pp. 159–170, 2014

17. Orozco, “Droplet impact on deep liquid pools: secondary droplets formation from Rayleigh jet break-up and crown splash”, University of Central Florida Orlando, Florida. film: anatomy of the splash”, 2015

18. Pan and Hung “Effects of Liquid and Surface Properties on Droplet-Film”, 48th AIAA Aerospace Sciences Meeting Including the New Horizons Forum and Aerospace Exposition, 2010

19. Tang, et al.,” Bouncing-to-Merging Transition in Drop Impact on Liquid Film: Role of Liquid Viscosity”, Langmuir, Vol. 34, pp. 2654-2662, 2018

20. Vander Wal, *et al*., “Droplets splashing upon films of the same fluid of various depths”, Experiments in Fluids, Vol. 40, pp. 33-52, 2006

21. Yang, *et al.*, “Effect of viscosity on motion of splashing crown in high speed drop impact”, Applied Mathematics and Mechanics -English Edition, Vol.38, pp.1709–1720, 2017

22. Yao, *et al.*, “Fragment *pdf*(d)s for drops impacting a thin liquid surface”, ILASS Americas 27th Annual Conference on Liquid Atomization and Spray Systems, 2017